Inter- and Intramolecular Experimental and Calculated Equilibrium Isotope Effects for (silox)$_2$(^{t}Bu$_3$SiND)TiR + RH (silox = ^{t}Bu$_3$SiO): Inferred Kinetic Isotope Effects for RH/D Addition to Transient (silox)$_2$Ti═NSi^{t}Bu$_3$

LeGrande M. Slaughter,[†] Peter T. Wolczanski,*[,†] Thomas R. Klinckman,[‡] and Thomas R. Cundari[‡]

Contribution from the Baker Laboratory, Department of Chemistry & Chemical Biology, Cornell University, Ithaca, New York 14853, and Computational Research on Materials Institute, Department of Chemistry, University of Memphis, Memphis, Tennessee 38152

Received January 10, 2000

Abstract: Intermolecular equilibrium isotope effects (EIEs) were measured (26.5 °C) and calculated for (silox)$_2$(^{t}Bu$_3$SiND)TiR$_D$ (**1**-ND-R$_D$) + R$_H$H ⇄ (silox)$_2$(^{t}Bu$_3$SiNH)TiR$_H$ (**1**-R$_H$) + R$_D$D: R$_H$H/R$_D$D = CH$_4$/CD$_4$, 2.00(6), calcd 1.88; C$_2$H$_6$/C$_2$D$_6$, 2.22(8), 1.93; ^{c}C$_3$H$_6$/^{c}C$_3$D$_6$, 1.71(4), 1.48; C$_2$H$_4$/C$_2$D$_4$, 1.41(11), 1.34; C$_6$H$_6$/C$_6$D$_6$, 1.22(7), 1.26; C$_7$H$_8$/C$_7$D$_8$ (50.0 °C), 1.59(6), 1.55. Related intramolecular EIEs for (silox)$_2$(^{t}Bu$_3$SiND)TiR′ (**1**-ND-R′) ⇄ (silox)$_2$(^{t}Bu$_3$SiNH)TiR (**1**-R) are provided: RH = R′D = CH$_3$D, 3.16(25), calcd 2.60; CH$_2$D$_2$, 1.13(8), 0.911; CHD$_3$, 0.389(20), 0.303; CH$_3$CD$_3$, 1.53(3), 1.44; 1,1-^{c}C$_3$H$_4$D$_2$, 2.58(6), 2.53; *trans*-HDC═CHD, 1.00(2), 1.00; 1,3,5-C$_6$H$_3$D$_3$, 1.273(4), 1.25; PhCH$_2$D (50.0 °C), 2.06(2), 1.98. Calculations of pertinent model complexes (e.g., (HO)$_2$(H$_2$N)TiR (**1′**-R)) generated the vibrational frequencies necessary to interpret the EIEs in terms of a statistical mechanics description utilizing gas-phase partition functions; EIE = SYM × MMI × EXC × EXP[−(ΔΔZPE/k_BT)]. The large MMI term in the intermolecular cases—a consequence of using perprotio vs perdeuterio small molecule substrates—is attenuated by EXC and EXP[−(ΔΔZPE/k_BT)] contributions derived from low-energy core vibrations. The EIEs are differentiated on the basis of the EXP[−(ΔΔZPE/k_BT)] term, with CH-based bending vibrations playing the major role. Substrate bending vibrations that are absent in intramolecular cases are primarily responsible for the greater intermolecular values. Using measured (or calculated) EIEs and kinetic isotope effects for 1,2-RH-elimination (KIE$_{elim}$) from **1**-R, KIE$_{addn}$ values for 1,2-RH-addition to putative intermediate (silox)$_2$Ti═NSi^{t}Bu$_3$ (**2**) were inferred via EIE = KIE$_{addn}$/KIE$_{elim}$. Extraordinary intermolecular KIE$_{addn}$ values ranging from ∼30 (CH$_4$/CD$_4$, C$_2$H$_6$/C$_2$D$_6$) to ∼9 (C$_6$H$_6$/C$_6$D$_6$) are consistent with previous mechanistic accounts and may be conventionally rationalized.

Introduction

Kinetic (KIE) and equilibrium isotope effects (EIE) provide mechanistic information that is critically dependent upon interpretation of their magnitudes. Conventional explanations of isotope effects rely on an assessment of zero-point energy (ZPE) differences between reactants and products (EIE) or transition-state species (KIE), the latter having one less antisymmetric vibration that is transformed into the reaction coordinate. For typical, relatively large isotopologues that differ by a small change in mass, the magnitude of an isotope effect is fairly interpreted on the basis of ZPE considerations—the dominant contributors to the reaction (EIE) or activation (KIE) enthalpy—provided the bonds being broken or changed in the reaction are characterized by vibrations that are substantial (>500 cm^{-1}). These caveats are typically heeded in experiments involving large organic molecules, where isotope effects commonly assess changes in C−H vs C−D bonds.[1−4]

In organometallic systems, isotope effects have proven instrumental in numerous mechanistic analyses, but recent investigations have suggested that interpretations based solely on ZPE differences are insufficient.[5−8] Employing calculational

[†] Cornell University.

[‡] University of Memphis.

(1) Carpenter, B. K. *Determination of Reaction Mechanisms*; Wiley-Interscience: New York, 1984.

(2) Melander, L.; Saunders, W. H., Jr. *Reaction Rates of Isotopic Molecules*; Wiley-Interscience: New York, 1980.

(3) *Isotope Effects in Chemical Reactions*; Collins, C. J., Bowman, N. S., Eds.; ACS Monograph No. 167; Van Nostrand Reinhold Co.: New York, 1970.

(4) Westheimer, F. H. *Chem. Rev.* **1961**, *61*, 265−273.

(5) Abu-Hasanayn, F.; Krogh-Jespersen, K.; Goldman, A. S. *J. Am. Chem. Soc.* **1993**, *115*, 8019−9023.

(6) (a) Rabinovich, D.; Parkin, G. *J. Am. Chem. Soc.* **1993**, *115*, 353−354. (b) Hascall, T.; Rabinovich, D.; Murphy, V. J.; Beachy, M. D.; Friesner, R. A.; Parkin, G. *J. Am. Chem. Soc.* **1999**, *121*, 11402−11417. Using eq 4, the authors' calculated EIE for (Me$_3$P)$_4$I$_2$WD$_2$ + H$_2$ ⇄ (Me$_3$P)$_4$I$_2$WH$_2$ + D$_2$ was 0.73, in good agreement with the experimentally observed 0.63(5).

(7) Bender, B. R. *J. Am. Chem. Soc.* **1995**, *117*, 11239−11246.

(8) Bender, B. R.; Kubas, G. J.; Jones, L. H.; Swanson, B. I.; Eckert, J.; Capps, K. B.; Hoff, C. D. *J. Am. Chem. Soc.* **1997**, *119*, 9179−9190.

(9) Bigeleisen, J.; Mayer, M. G. *J. Chem. Phys.* **1947**, *15*, 261−267.

(10) (a) Walsh, P. J.; Hollander, F. J.; Bergman, R. G. *Organometallics* **1993**, *12*, 3705−3723. (b) Lee, S. Y.; Bergman, R. G. *J. Am. Chem. Soc.* **1995**, *117*, 5877−5878.

(11) Cummins, C. C.; Schaller, C. P.; Van Duyne, G. D.; Wolczanski, P. T.; Chan, E. A.-W.; Hoffmann, R. *J. Am. Chem. Soc.* **1991**, *113*, 2985−2994.

(12) (a) Schaller, C. P.; Cummins, C. C.; Wolczanski, P. T. *J. Am. Chem. Soc.* **1996**, *118*, 591−611. (b) Schaller, C. P., Ph.D. Thesis, Cornell University, 1993.

(13) Schaller, C. P.; Bonanno, J. B.; Wolczanski, P. T. *J. Am. Chem. Soc.* **1994**, *116*, 4133−4134.

10.1021/ja000112q CCC: $19.00
Published on Web 08/23/2000

Scheme 1

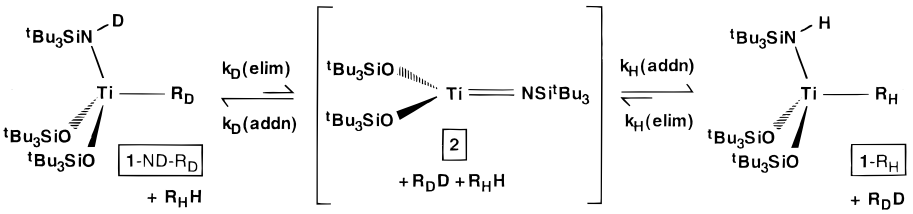

R_H = CH_3 (Me), CH_2CH_3 (Et), $^c(CH_2)_3$ (^{c}Pr), $CH{=}CH_2$ (Vy), C_6H_5 (Ph), $CH_2C_6H_5$ (Bz)
R_D = CD_3, CD_2CD_3, $^c(CD_2)_3$, $CD{=}CD_2$, C_6D_5, $CD_2C_6D_5$

Scheme 2

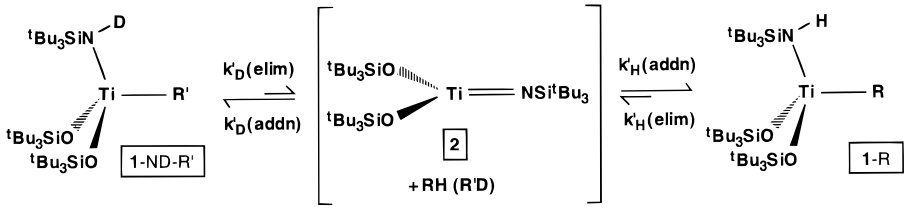

RH = R'D = CH_3D, CH_2CD_2, CHD_3, CH_3CD_3, $^c(CH_2CH_2CD_2)$,
trans-CHD=CHD, 1,3,5-$C_6H_3D_3$, $H_2DCC_6H_5$

models that complemented experiments on Vaska's complex,[5] Goldman et al. clearly showed that the EIE (eqs 1−3) pertaining to H_2 (R_H = H) vs D_2 (R_D = D) oxidative addition could only be properly interpreted by viewing the full statistical mechanical treatment of the isotopic equilibrium.[9]

$$L_nM + R_HH \overset{K_H}{\rightleftharpoons} L_nM(R_H)H \quad (1)$$

$$L_nM + R_DD \overset{K_D}{\rightleftharpoons} L_nM(R_D)D \quad (2)$$

$$L_nM(R_D)D + R_HH \overset{K_H/K_D}{\rightleftharpoons} L_nM(R_H)H + R_DD \quad (3)$$

$$K_H/K_D = \mathrm{EIE} = \mathrm{SYM} \times \mathrm{MMI} \times \mathrm{EXC} \times \mathrm{EXP}[-(\Delta\Delta\mathrm{ZPE}/k_BT)] \quad (4)$$

$$\frac{Q_{tr}(L_nM(R_H)H)Q_{tr}(R_DD)Q_{rot}(L_nM(R_H)H)Q_{rot}(R_DD)}{Q_{tr}(L_nM(R_D)D)Q_{tr}(R_HH)Q_{rot}(L_nM(R_D)D)Q_{rot}(R_HH)} = \mathrm{SYM} \times \mathrm{MMI} \quad (5)$$

$$\frac{Q_{vib}(L_nM(R_H)H)Q_{vib}(R_DD)}{Q_{vib}(L_nM(R_D)D)Q_{vib}(R_HH)} = \mathrm{EXC} \quad (6)$$

$$\mathrm{EXP}[-\{(\mathrm{ZPE}(L_nM(R_H)H) - \mathrm{ZPE}(L_nM(R_D)D)) + (\mathrm{ZPE}(R_DD) - \mathrm{ZPE}(R_HH))\}/k_BT] = \mathrm{EXP}[-(\Delta\Delta\mathrm{ZPE}/k_BT)] \quad (7)$$

The experimentally observed value of 0.55 was quite close to the 0.46 calculated from eq 4, which represents the partition function product/reactant ratios as given in eqs 5−7, with gas-phase Q's: $Q_{tr} = (2\pi MkT)^{3/2}/h^3$, $Q_{rot} = \{\pi(8\pi^2k_BT)^3I_AI_BI_C\}^{1/2}/\sigma h^3$, $Q_{vib} = \Pi_i^{3n-6}(1 - \exp(-h\upsilon_i/k_BT))^{-1}$, $\mathrm{ZPE} = \Sigma_i^{3n-6}(h\upsilon_i/2)$, M = molecular mass, k_B = Boltzmann constant, T = temperature (K), h = Planck's constant, I = moment of inertia, σ = symmetry number, and υ_i = vibrational frequency of normal mode i. For convenient interpretation, the symmetry numbers have been separated from the rotational partition function ratio as the SYM term in eqs 4 and 5, and the remaining Q_{rot} components have been combined with the translational partition function ratio to formulate the mass moment of inertia (MMI) term. Interpretations of EIE and KIE values herein will be conducted within the textbook framework provided by eq 4.[1−4,9]

During the course of investigating hydrocarbon activations involving 1,2-R_HH-addition to transient metal imido complexes,[10] $X_{3-n}M(=NSi^tBu_3)_n$ (X = $HNSi^tBu_3$, M = Ti, n = 1;[11] M = Zr, Hf, n = 1;[12,13] M = V,[14] Ta,[15] n = 2; M = W,[16] n = 3; X = OSi^tBu_3, M = Ti, n = 1 (2)),[17] KIE measurements helped address the mechanism of 1,2-R_HH-elimination from hydrocarbyl precursors such as (silox)$_2$(^{t}Bu$_3$SiNH)TiR_H (**1**-R_H). In this titanium system, equilibrium studies involving **1**-R_H + R′$_H$H established the relative ground-state energies of **1**-R_H, and suggested that equilibrium isotope effect measurements could be made in the context of examining the details of C−H/D activation by metal imido complexes. Herein are presented observed and calculated EIE measurements in the titanium system, which, when combined with measured KIEs of 1,2-R_HH/D-elimination,[17] afford estimates of KIEs of 1,2-R_HH/D-addition.

Results

The (silox)$_2$(^{t}Bu$_3$SiNH)TiR_H (1-R_H) System. 1. Intermolecular EIE. The equilibrium isotope effect experiments that parallel the general reactions of eqs 1−3 are expressed as the 1,2-R_HH- and 1,2-R_DD-elimination and -addition reactions in Scheme 1, with R_H and R_D referring to perprotio and perdeuterio hydrocarbyls, respectively. The EIE is given as the ratio of addition to elimination k_H/k_D's as shown in eq 8, and in terms

(14) de With, J.; Horton, A. D. *Angew. Chem., Int. Ed. Engl.* **1993**, *32*, 903−905.
(15) Schaller, C. P.; Wolczanski, P. T. *Inorg. Chem.* **1993**, *32*, 131−144.
(16) Schafer, D. F., II; Wolczanski, P. T. *J. Am. Chem. Soc.* **1998**, *120*, 4881−4882.
(17) Bennett, J. L.; Wolczanski, P. T. *J. Am. Chem. Soc.* **1997**, *119*, 9, 10696−10719.
(18) We thank Prof. Alan S. Goldman for bringing this argument to our attention.
(19) (a) *IUPAC Solubility Data Series*; Pergamon Press: New York, Vol. 9, pp 138−149 (ethane); Vol. 27−28, pp 450−469 (methane). (b) Drymond, J. H. *J. Phys. Chem.* **1967**, *71*, 1829−1831 (cyclopropane). (c) Krauss, W.; Gestrich, W. *Chem. Technol.* **1977**, *6* (12), 513−516 (ethylene).

of the concentrations of the perprotio and perdeuterio hydrocarbyl complexes and hydrocarbons as indicated in eq 9.

$$\mathrm{EIE} = \frac{K_\mathrm{H}}{K_\mathrm{D}} = \frac{\{k_\mathrm{D}(\mathrm{elim})\}\{k_\mathrm{H}(\mathrm{addn})\}}{\{k_\mathrm{H}(\mathrm{elim})\}\{k_\mathrm{D}(\mathrm{addn})\}} \quad (8)$$

$$\mathrm{EIE} = \frac{K_\mathrm{H}}{K_\mathrm{D}} = \frac{[\mathbf{1}\text{-}\mathrm{R_H}][\mathrm{R_D D}]}{[\mathrm{R_H H}][\mathbf{1}\text{-}\mathrm{ND\text{-}R_D}]} \quad (9)$$

Equations 4−7, with $L_nM(R_H)H$ representing **1**-R_H, include partition functions of the substrates and are applicable in the intermolecular cases.

2. Intramolecular EIE. A related *intramolecular* EIE is described by Scheme 2, and the definitions of $K'_\mathrm{H} = k'_\mathrm{H}(\mathrm{addn})/k'_\mathrm{H}(\mathrm{elim})$ and $K'_\mathrm{D} = k'_\mathrm{D}(\mathrm{addn})/k'_\mathrm{D}(\mathrm{elim})$ are similar to the intermolecular case in Scheme 1, with RH (R′D) referring to a partially deuterated hydrocarbon. In contrast to the intermolecular cases, measurements of the metal-containing isotopomer concentrations, but not $[H_xD_yC_z]$, are consequential to the EIE (eq 10).

$$\mathrm{EIE} = \frac{K_\mathrm{H}}{K_\mathrm{D}} = \frac{[\mathbf{1}\text{-R}]}{[\mathbf{1}\text{-ND-R}']} \quad (10)$$

$$\mathrm{EIE} = \frac{Q_\mathrm{tr}(\mathbf{1}\text{-R})Q_\mathrm{rot}(\mathbf{1}\text{-R})Q_\mathrm{vib}(\mathbf{1}\text{-R})}{Q_\mathrm{tr}(\mathbf{1}\text{-ND-R}')Q_\mathrm{rot}(\mathbf{1}\text{-ND-R}')Q_\mathrm{vib}(\mathbf{1}\text{-ND-R}')} \times \mathrm{EXP}[-\{\mathrm{ZPE}(\mathbf{1}\text{-R}) - \mathrm{ZPE}(\mathbf{1}\text{-ND-R}')\}/k_\mathrm{B}T] \quad (11)$$

This difference has a significant consequence on the magnitude and interpretation of isotope effects; partition functions that describe the EIE are comprised solely of components pertaining to the metal complexes, while eqs 4−7 contain partition functions of the hydrocarbons.

3. Gas-Phase Partition Functions. To interpret the EIE measurements, calculations of the partition functions in eq 4 were conducted pertaining to the gas phase. While the validity of using the functional forms for gas phase Q_tr, Q_rot, and Q_vib to represent their solution counterparts may be questioned, calculation of an EIE via eq 4 only requires that the various partition function ratios have the same $M^{3/2}$ (translation), $I^{1/2}$ (rotation), and exponential υ (EXC, ZPE) dependencies. As an illustration, consider the problem of solubilities described by eqs 12−14.[18]

$$\mathrm{R_H H(g)} \overset{K_\mathrm{H}}{\rightleftharpoons} \mathrm{R_H H(soln)} \quad (12)$$

$$\mathrm{R_D D(g)} \overset{K_\mathrm{D}}{\rightleftharpoons} \mathrm{R_D D(soln)} \quad (13)$$

$$\mathrm{R_H H(g)} + \mathrm{R_D D(soln)} \overset{K_\mathrm{H}/K_\mathrm{D}}{\rightleftharpoons} \mathrm{R_D D(g)} + \mathrm{R_H H(soln)} \quad (14)$$

For the case of CH_4 and CD_4, the $Q_\mathrm{rot}(CD_4(g))/Q_\mathrm{rot}(CH_4(g))$ ratio is 2.83, and $Q_\mathrm{trans}(CD_4(g))/Q_\mathrm{trans}(CH_4(g))$ is 1.40. Since the EXC and ZPE terms could reasonably be considered nearly equivalent in the gas and solution phases, $Q_\mathrm{rot}(CD_4(soln))/Q_\mathrm{rot}(CH_4(soln))$ and $Q_\mathrm{trans}(CD_4\ (soln))/Q_\mathrm{trans}(CH_4\ (soln))$ must also be 2.83 and 1.40 if CH_4 and CD_4 have the same solubilities. The solubilities of CH_4 and CD_4 are effectively equivalent, as are the other hydrocarbon isotopologues (i.e., in eq 14, $K_H/K_D \approx 1$);[13,19] hence, the rotational and translational partition functions for the gas- and solution-phase species must have the same mass and moment of inertia dependencies. Gas-phase partition function ratios are therefore considered valid approximations of their solution-phase counterparts in this study.

4. (HO)$_2$(H$_2$N)TiR$_H$ (1′-R$_H$) Models. The various partition functions for hydrocarbon substrates can be reliably calculated by modern methods. In addition, $Q_\mathrm{rot}(\mathbf{1}\text{-R}_H)/Q_\mathrm{rot}(\mathbf{1}\text{-ND-R}_D)$, $Q_\mathrm{rot}(\mathbf{1}\text{-R})/Q_\mathrm{rot}(\mathbf{1}\text{-ND-R}')$, $Q_\mathrm{trans}(\mathbf{1}\text{-R}_H)/Q_\mathrm{trans}(\mathbf{1}\text{-ND-R}_D)$, and $Q_\mathrm{trans}(\mathbf{1}\text{-R})/Q_\mathrm{trans}(\mathbf{1}\text{-ND-R}')$ can be safely approximated as 1.00, since changes in the mass and moment of inertia that occur upon deuteration of these transition metal compounds are effectively inconsequential. The calculation of vibrational frequencies that need to be utilized in the excitation (EXC, eq 6) and zero-point energy (ZPE, eq 7) terms of eq 4 is of critical importance. Under the best circumstances, experimental frequencies can be used, but this requires careful analysis and assignment of infrared spectral absorptions. Bender took advantage of experimental frequencies of $[(OC)_4Os]_2(\mu\text{-}\eta^1,\eta^1\text{-}C_2H_4/C_2D_4)$ in calculating the EIE for ethylene binding,[7] but modes describing the diosmametallacycle were well separated from the carbonyl and metal−carbonyl-based absorptions in the infrared spectrum. In **1**-R_H and its isotopologues, significant overlap exists between frequencies derived from the OSi^{t}Bu$_3$ and NHSi^{t}Bu$_3$ ligands and those of the hydrocarbyl. In a previous system, (^{t}Bu$_3$SiNH)$_3$ZrCH$_3$, (^{t}Bu$_3$SiND)$_3$ZrCH$_3$, (^{t}Bu$_3$SiNH)$_3$-ZrCD$_3$, and ((d_9-^{t}Bu)$_3$SiNH)$_3$ZrCH$_3$ were prepared in an effort to distinguish vibrational frequencies, but reliable assignments could not be ascertained.[12] As a consequence of this experience and corresponding calculations, modern ab initio quantum mechanical methods were sought in order to generate a set of frequencies that would properly describe the core of **1**-R_H.

Effective core potential calculations were previously employed to successfully track experimental 1,2-RH-eliminations[12,17] with models $(H_2N)_3MR_H$ (M = Ti, Zr, Hf) and $(H_2N)_2(HN{=})MR_H$ (M = V, Nb, Ta),[20−23] and to estimate alkane binding via $(H_2N)_{3-x}(HN{=})_xM$ ($x = 1$, M = Ti, Zr, Hf; $x = 2$, M = V, Nb, Ta; $x = 3$, M = W, Re^+).[24,25] In keeping with this effort, $(HO)_2(HNH)TiR_H$ (**1′**-R_H) models were calculated as computational analogues to (silox)$_2$(^{t}Bu$_3$SiNH)TiR_H (**1**-R_H). Figure 1 illustrates the seven hydrocarbyl and metallacyclic complexes investigated and is accompanied by an abbreviated chart of some pertinent bond distances and angles (Table 1). The elimination of the siloxide and silamide moieties in the models served two purposes: frequencies corresponding to the ancillary ligands were removed while the critical core vibrations were preserved, and the simplified models enabled reasonably swift calculations for all RH, in part because numerous conformations of the ancillary groups or more complex analogues (e.g., −OSiMe$_3$) were avoided. Most of the features of the models proved satisfactory. For example, in the true complex (**1**-R_H), the tri-*tert*-butylsilamide is expected to be planar,[12,17] and each **1′**-RH model contains amide TiNH angles of ∼125° and an accompanying HNH angle of ∼110°. Although no structural details have been obtained, the models were deemed acceptable and the calculated EIEs, factored into their components according to eq 4, are tabulated in Table 2.

Measurements of EIE. 1. Intermolecular. Prior to measurement of each intermolecular EIE shown in Scheme 1, a simulation of the approach to equilibrium was made by using the known 1,2-RH-elimination rates (k_H(elim)) for each (silox)$_2$-

(20) Cundari, T. R. *J. Am. Chem. Soc.* **1992**, *114*, 10557−10563.
(21) Cundari, T. R.; Gordon, M. S. *J. Am. Chem. Soc.* **1993**, *115*, 4210−4217.
(22) Cundari, T. R. *Organometallics* **1994**, *13*, 2987−2994.
(23) Cundari, T. R. *Organometallics* **1993**, *12*, 4971−4978.
(24) Cundari, T. R. *Organometallics* **1993**, *12*, 1998−2000.
(25) Cundari, T. R. *Inorg. Chem.* **1998**, *37*, 5399−5401.

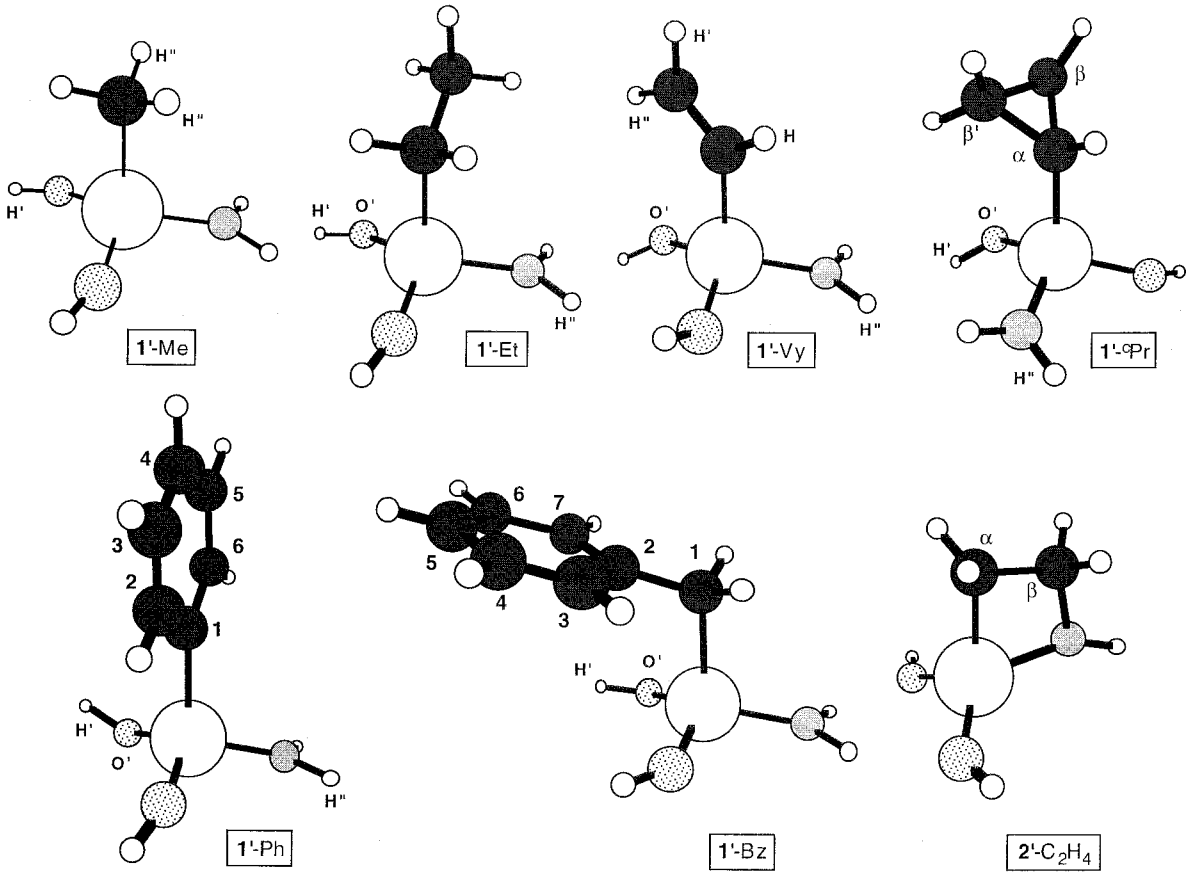

Figure 1. Calculated models $(HO)_2(H_2N)TiR$ (**1′**-R) of $(silox)_2(^tBu_3SiNH)TiR$ (**1**-R); pertinent bond distances and angles are given in Table 1.

$(^tBu_3SiNH)TiR_H$ (**1**-R_H), guessing various k_D(elim) for $(silox)_2(^tBu_3SiND)TiR_D$ (**1**-ND-R_D), and generating k_H(addn) and k_D(addn) by using the estimated standard free energy of $(silox)_2Ti{=}NSi^tBu_3$ (**2**) relative to **1**-R_H.[17] Times varied considerably, from ~2 d for **1**-C_6H_5 + C_6D_6 to ~30 d for **1**-CH_3 + CD_4, and each set of samples was analyzed at least twice to ensure that equilibrium had been achieved. Due to the thermal instability of many **1**-R_H/**1**-ND-R_D, it became convenient to prepare equilibrium mixtures by generating $(silox)_2Ti{=}NSi^tBu_3$ (**2**) in the presence of R_HH and R_DD via 1,2-^{c}PeH-elimination from $(silox)_2(^tBu_3SiNH)Ti^cPe$ (**1**-^{c}Pe, eq 15) at 26.5(3) °C. Neither cyclopentane nor solvent cyclohexane is a serious

$$\underset{\textbf{1}\text{-}^c\text{Pe}}{(silox)_2(^tBu_3SiNH)Ti^cPe} \overset{C_6H_{12}}{\underset{\Delta}{\rightleftharpoons}} \underset{\textbf{2}}{(silox)_2Ti{=}NSi^tBu_3} + {}^cPeH \quad (15)$$

competitor for **2** in comparison to the substrates of interest, and their presence was not experimentally significant.

The EIE expression given in eq 9 reveals a simple way of measuring an intermolecular EIE. Integration of the ^{1}H NMR signals of **1**-R_H and R_HH afforded [**1**-R_H]/[R_HH], integration of ^{2}H NMR signals of R_DD and **1**-ND-R_D gave [R_DD]/[**1**-ND-R_D], and the product of these ratios provided a direct measure of the EIE for each substrate pair. Details of the NMR analyses are given in the Experimental Section, and the EIE_{obs} values are given in Table 2.

2. Intramolecular. The intramolecular experiments were initiated by generating **2** via eq 15 in the presence of RH = R′D in cyclohexane or C_6D_{12}. Approaches to equilibrium in the intramolecular cases were again simulated prior to each experiment (e.g., ~37 d for CH_3D). Equation 10 shows that direct integration of the [**1**-R] to [**1**-ND-R′] ratio directly supplied the EIE in the intramolecular case. This measurement was conducted by ^{1}H NMR spectroscopy, except for the methane cases, which were analyzed by ^{2}H NMR spectroscopy. It follows from eq 11 that the intramolecular EIE is isotopologue and isotopomer specific. For a given isotopologue (e.g., $C_2H_3D_3$) there exist a number of isotopomers (e.g., H_3CCD_3, H_2DCCHD_2) that are pertinent counterparts to the related intermolecular substrates. For the case of methane, all isotopologues (e.g., CH_3D, CH_2D_2, and CD_3H) were examined, while a single isotopomer of one isotopologue was chosen in the other instances. The experimental EIEs are listed along with their calculated counterparts in Table 2. Calculations showed that while an EIE is specific to an isotopomer, only small differences among isotopomers or even isotopologues were evident. On this basis, inclusion of other intramolecular cases was not justified.

Kinetic Isotope Effect (KIE) Measurements. Direct measurement of k_H(elim)/k_D(elim), the KIE for 1,2-R_HH/D-elimination, was accomplished by monitoring the disappearance of the hydrocarbyl, $(silox)_2(^tBu_3SiNH)TiR_H$ (**1**-R_H), and its amide-deuterated isotopologue, **1**-ND-R_H, in tandem by ^{1}H NMR spectroscopy. The intermediate $(silox)_2Ti{=}NSi^tBu_3$ (**2**) must be irreversibly trapped for clean first-order kinetics. It was typically sufficient to run the reactions in C_6D_6, where formation of $(silox)_2(^tBu_3SiND)TiC_6D_5$ (**1**-ND-C_6D_5) was effectively irreversible. Disappearance rates of **1**-CH_3 vs **1**-ND-CH_3, **1**-CH_2Ph vs **1**-ND-CH_2Ph, and **1**-C_6H_5 vs **1**-ND-C_6D_5 have been measured previously using this method,[17] and KIEs for the ethyl, cyclopropyl, and vinyl cases were similarly measured: **1**-Et vs **1**-ND-Et, k_H(elim)/k_D(elim) = 14.3(7); **1**-^{c}Pr vs **1**-ND-^{c}Pr, k_H(elim)/k_D(elim) = 9.0(5); **1**-Vy vs **1**-ND-Vy, k_H(elim)/k_D(elim)

Table 1. Abbreviated Listing of Structural Parameters for (HO)$_2$(H$_2$N)TiR (**1′**-R) and (HO)$_2$(HN)TiCH$_2$CH$_2$ (**2′**-CH$_2$CH$_2$) Determined from RHF/SBK(d) Calculations[a,b]

1′-R, d(Å)	TiO	TiN	TiC	OH	NH	CH	CC/N
1′-CH$_3$	1.80	1.90	2.08	0.95	1.02	1.80	
1′-C$_2$H$_5$	1.80	1.90	2.08	0.95	1.02	1.10	1.54
1′-^{c}C$_3$H$_5$	1.81	1.90	2.06	0.96	1.02	1.10 α	1.53 αβ
				0.95 H′		1.09 β	1.51 $\beta\beta$
1′-CH=CH$_2$	1.80	1.89	2.08	0.96	1.02	1.10 H,H′	1.35
						1.09 H″	
1′-C$_6$H$_5$	1.80	1.89	2.09	0.95	1.02	1.09	1.41 C^{1}C^2,C^{2}C^3,C^{4}C^5
				0.96 H′			1.40 C^{3}C^4,C^{5}C^6
							1.42 C^{1}C^6
1′-CH$_2$Ph	1.80	1.89	2.10	0.95	1.02	1.10 α	1.51 C^{1}C^2
							1.41 C^{2}C^3,C^{4}C^5,C^{5}C^6,C^{2}C^7
							1.40 C^{3}C^4,C^{6}C^7
2′-H$_2$CCH$_2$	1.82	1.86	2.07	0.96	1.01	1.10	1.56 CC
							1.49 CN

1′-R, angles (deg)	OTiO	OTiN	OTiC	NTiC	TiCC	TiOH	TiNH	TiCH	HNH	HCH
1′-CH$_3$	120.3	110.6	103.9	106.1		157.2	125.2	109.9	109.5	108.4
						157.5 H′		110.8 H″		108.5 H″
1′-C$_2$H$_5$	120.8	110.6	103.8	105.7	116.6	157.1	125.4	105.6 α	109.4	106.4 α
		111.2 O′	103.0 O′			160.9 O′	125.2 H″	106.9 α		
1′-^{c}C$_3$H$_5$	118.8	109.0	105.3	107.5	122.0 β	138.3	125.8	115.3	109.6	
		112.1 O′	103.2 O′		120.9 β′	144.8 O′	124.7 H″			
1′-CH=CH$_2$	115.8	111.2	104.8	107.2	126.2	137.6	124.7	118.2	109.5	
			106.0			141.9 O′	125.4 H″			
1′-C$_6$H$_5$	118.1	111.6	104.5	108.5	121.8 C^2	144.8	124.9		109.7	
		108.1	105.5 O′		121.2 C^6	136.2 O′	125.4 H″			
1′-CH$_2$Ph	121.4	110.5	103.5	105.8	110.9	143.8	125.2	107.8	109.6	107.8
						144.4				
2′-H$_2$CCH$_2$	113.4	118.2	113.0	75.4	85.4	136.2	148.7	116.6		109.9 α
					95.1 NC					108.6 β
					104.1 CCN					

[a] All distances and angles refer to the models **1′**-R and **2′**-CH$_2$CH$_2$ portrayed in Figure 1. [b] If only one distance or angle is given, the same value was calculated for other distances or angles of this type.

Table 2. Experimentally Observed and Calculated Intermolecular and Intramolecular Equilibrium Isotope Effects[a,b]

substrates	EIE$_{obs}$	EIE$_{calc}$	= SYM	x MMI[c]	× EXC	× EXP[−(ΔΔZPE/k_BT)]
Intermolecular (**1**-ND-R$_D$ + R$_H$H ⇄ **1**-R$_H$ + R$_D$D)						
1-ND-CD$_3$ + CH$_4$ ⇄ **1**-CH$_3$ + CD$_4$	2.00(6)	1.88	1	3.95	0.500	0.950
1-ND-C$_2$D$_5$ + C$_2$H$_6$ ⇄ **1**-C$_2$H$_5$ + C$_2$D$_6$	2.22(8)	1.93	1	2.69	0.551	1.299
1-ND-^{c}C$_3$D$_5$ + ^{c}C$_3$H$_6$ ⇄ **1**-^{c}C$_3$H$_5$ + ^{c}C$_3$D$_6$	1.71(4)	1.48	1	2.04	0.616	1.177
1-ND-DCCD$_2$ + H$_2$CCH$_2$ ⇄ **1**-HCCH$_2$ + D$_2$CCD$_2$	1.41(11)	1.34	1	2.45	0.591	0.924
1-ND-C$_6$D$_5$ + C$_6$H$_6$ ⇄ **1**-C$_6$H$_5$ + C$_6$D$_6$	1.22(7)	1.26	1	1.49	0.702	1.200
1-ND-C$_7$D$_7$ + C$_7$H$_8$ ⇄ **1**-C$_7$H$_7$ + C$_7$D$_8$[d,e]	1.59(6)	1.55	1	1.52	0.822	1.240
2-D$_2$CCD$_2$ + H$_2$CCH$_2$ ⇄ **2**-HCCH$_2$ + D$_2$CCD$_2$-[f]	0.879(11)	0.893	1	2.45	0.766	0.476
Intramolecular (**1**-ND-R′ ⇄ **1**-R)						
1-ND-CH$_3$ ⇄ **1**-CH$_2$D[g]	3.16(25)	2.60	3	1.00	0.956	0.908
1-ND-CDH$_2$ ⇄ **1**-CHD$_2$	1.13(8)	0.911	1	1.00	0.934	0.976
1-ND-CHD$_2$ ⇄ **1**-CD$_3$[h]	0.389(20)	0.303	1/3	1.00	0.925	0.982
1-ND-CD$_2$CH$_3$ ⇄ **1**-CH$_2$CD$_3$	1.53(3)	1.44	1	1.00	0.969	1.482
1-ND-^{c}(CDCH$_2$CH$_2$) ⇄ **1**-^{c}(CHCH$_2$CD$_2$)	2.58(6)	2.53	2	1.00	0.869	1.457
1-ND-*trans*-HC=CHD ⇄ **1**-*trans*-CD=CHD	1.00(2)	1.00	1	1.00	0.931	1.075
1-ND-(3,5-C$_6$H$_3$D$_2$) ⇄ **1**-(2,4,6-C$_6$H$_2$D$_3$)	1.273(4)	1.25	1	1.00	0.855	1.460
1-ND-CH$_2$Ph ⇄ **1**-CHDPh[d,e]	2.06(2)	1.98	2	1.00	0.867	1.143

[a] All terms refer to eq 4, with definitions provided in the text; the EXC and EXP[−(ΔΔZPE/k_BT)] terms were calculated using frequencies from the models **1′**-R$_H$, **1′**-ND-R$_D$, **1**-R, and **1**-ND-R′. [b] 26.5(3) °C (exptl) and 24.8 °C (calcd) except for the toluene cases. [c] The MMI term assumes Q_{rot}(**1**-R$_H$)/Q_{rot}(**1**-ND-R$_D$) = 1.00 and Q_{tr}(**1**-R$_H$)/Q_{tr}(**1**-ND-R$_D$) = 1.00; hence it is determined solely by Q_{rot}(R$_D$D)/Q_{rot}(R$_H$H) and Q_{tr}(R$_D$D)/Q_{tr}(R$_H$H) in the intermolecular case. The MMI term assumes Q_{rot}(**1**-R)/Q_{rot}(**1**-ND-R′) = 1.00 in the intramolecular case. [d] Refers to benzyl activated products, **1**-CH$_2$Ph and isotopologues. [e] 50.0(3) °C (exptl) and 50.0 °C (calcd). [f] Refers to metallacylic product (silox)$_2$(^{t}Bu$_3$SiN)TiCH$_2$CH$_2$ (**2**-C$_2$H$_4$) and its isotopologue, **2**-D$_2$CCD$_2$. [g] EIE$_{obs}$/SYM = 1.05; EIE$_{calc}$/SYM = 0.867. [h] EIE$_{obs}$/SYM = 1.17; EIE$_{calc}$/SYM = 0.909.

= 7.8(4). As a test for the direct measurement of secondary effects, the KIE for **1**-CH$_3$ vs **1**-NH-CD$_3$ was determined to be 1.07(10) or 1.02(3)/D. On the basis of this and previous measurements in a related Zr system,[12] secondary KIEs were thought to be ∼1 and within experimental error; hence, no further effort was made toward direct measurement.

Discussion

Observed and Calculated EIEs: Generalities. 1. The Model and Experiment. The observed intermolecular and intramolecular equilibrium isotope effects (EIEs) and their calculated, factored counterparts are given in Table 2. Values for EIE$_{obs}$ and EIE$_{calc}$ pertaining to the various substrates are reasonably comparable. In the worst cases—the intramolecular methane isotopologues—the calculated EIEs are low by ∼20%. Considering experimental difficulties and the liberties taken in modeling (silox)$_2$(^{t}Bu$_3$SiNH)TiR$_H$ (**1**-R$_H$) by the much simpler (HO)$_2$(HNH)TiR$_H$ (**1′**-R$_H$), it is gratifying to note that the ^{t}Bu-rich periphery does not appear to manifest a great deal of influence on changes within the core of the molecules; i.e., the models are appropriate.

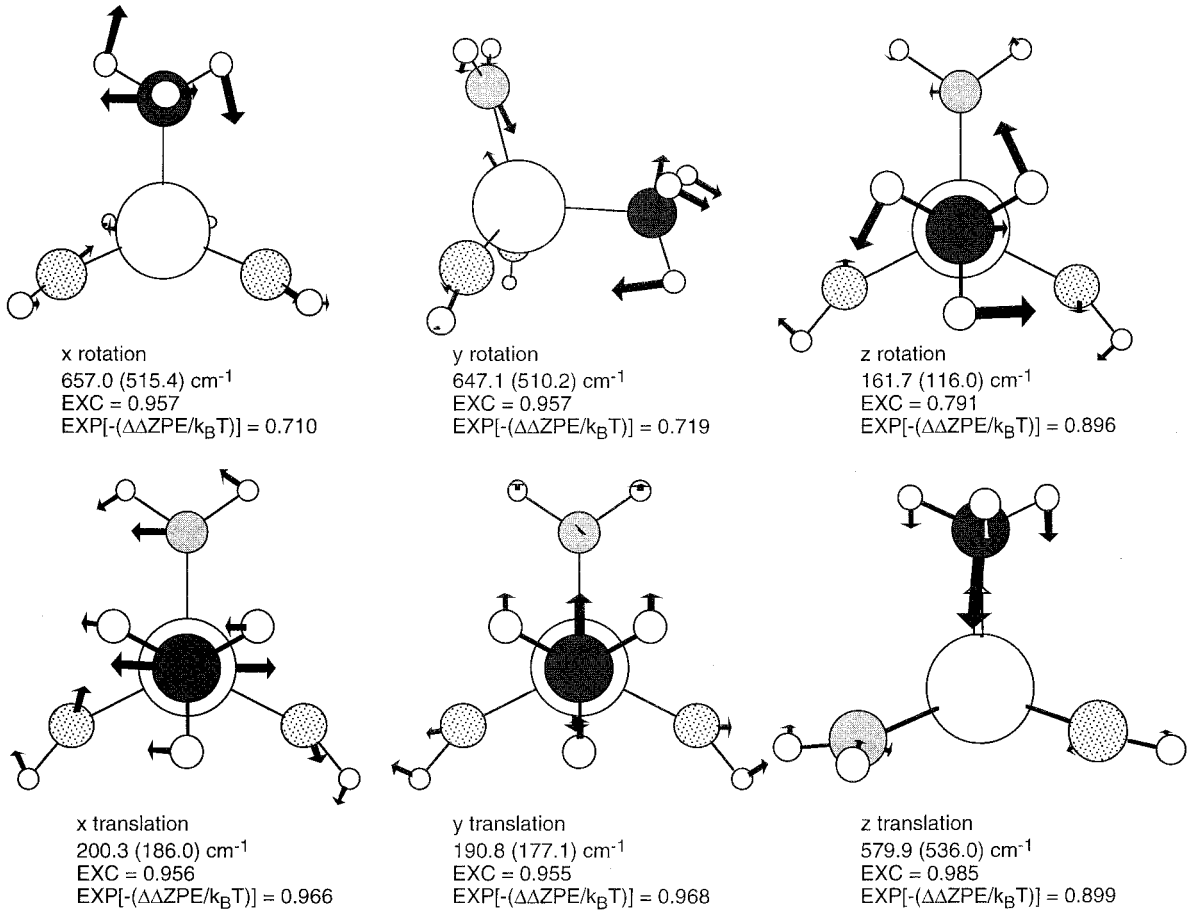

Figure 2. Core vibrational remnants of methane rotation and translation in **1′**-CH_3 (**1′**-ND-CD_3) and their uncorrelated contributions to EXC and EXP[$-(\Delta\Delta ZPE/k_BT)$].

Values of the calculated EIEs are lower than those observed in virtually every case. It is possible that a systematic error in the calculated values exists—or that the observed values are similarly subject to an experimental error that renders them high. In terms of the calculations, partition function ratios based on the vibrational frequencies are the most likely sources of error, because the MMI ratio is simply dependent on mass and moment of inertia, and these quantities are easily calculated. The vibrational frequencies in quantum calculations follow from the harmonic oscillator approximation and are often "scaled" when experimental vibrational data permit comparison. While a scale factor >1 would shift the EIE_{calc} closer to the observed EIEs, a significant multiplier would be needed, and there is little precedent for its utilization for the purposes herein. Since scaling would be applied to both the protiated and deuterated species in assessing eq 4, a 10% change in vibrational frequencies only translates into ~6% change in EIE_{calc}. Scaling corrections were not employed because such minor changes were not deemed important in interpreting the EIEs.[26−28]

A second possibility concerns the viability of the harmonic oscillator in approximating low frequencies. Consider the intermolecular methane case: **1′**-ND-CD_3 + CH_4 ⇄ **1′**-CH_3 + CD_4. The MMI term is attenuated by an EXC term of 0.500 whose composition (Table 2) reveals the importance of remnants of rotation (vide infra). A single vibration of **1′**-CH_3 (**1′**-ND-CD_3) at 161.7 (116.0) cm^{-1} contributes 0.791 toward the EIE_{calc}. The illustration in Figure 2 (labeled *z* rotation) clearly underscores the relationship of this HCTiN torsion to the rotation of free methane. The low frequency of this torsion—chosen because it was the largest single low-frequency contributor to EXC terms in all the **1′**-R_H examples discussed—proved to be a valuable test of the harmonic oscillator approximation. A hindered rotor approximation developed by Truhlar[29] estimates the total vibrational partition function for a hindered rotor (Q_{hin}; Q as defined here is the product of the EXC and EXP[$-(\Delta\Delta ZPE/k_BT)$] contributions, eq 16) by correcting the partition function derived from the harmonic oscillator approximation (Q_{har}, eq 17) using an interpolation function f_i (eq 18) involving the free rotor partition function (Q_{fr}, eq 19).

$$Q_{hin} = Q_{har}\, f_i \tag{16}$$

$$Q_{har} = \exp(-h\nu_i/2k_BT)/(1 - \exp(-h\nu_i/k_BT)) \tag{17}$$

$$f_i = \tanh(Q_{fr}(h\nu_i/k_BT)) \tag{18}$$

$$Q_{fr} = (Ik_BT)^{1/2}/\sigma h;$$
$$\sigma = \text{symmetry number}, I = \text{moment of inertia} \tag{19}$$

Computing a more realistic vibrational contribution to the EIE from the methyl torsion mode of **1′**-CH_3 and **1′**-ND-CD_3 resulted in negligible changes in individual Q's, as well as the ratio of Q's; Q_{har}(**1′**-CH_3) = 1.247, Q_{hin}(**1′**-CH_3) = 1.240; Q_{har}(**1′**-CH_3)/Q_{har}(**1′**-ND-CD_3) = 0.7085; Q_{hin}(**1′**-CH_3)/Q_{hin}(**1′**-ND-CD_3) =

(26) Cundari, T. R.; Raby, P. D. *J. Phys. Chem.* **1997**, *101*, 5783−5788.
(27) Harris, N. J. *J. Phys. Chem.* **1995**, *99*, 14689−14699.
(28) (a) Rauhut, G.; Pulay, P. *J. Phys. Chem.* **1995**, *99*, 3093−3100. (b) Flock, M.; Ramek, M. *Int. J. Quantum Chem., Quantum Chem. Symp.* **1993**, *27*, 331−336. (c) Lee, J. Y.; Hahn, O.; Lee, S. J.; Mhin, B. J.; Lee, M. S.; Kim, K. S. *J. Phys. Chem.* **1995**, *99*, 2262−2266.
(29) Truhlar, D. G. *J. Comput. Chem.* **1991**, *12* (2), 266−270.

0.7086.[30] The treatment suggests that the harmonic oscillator approximation is a reasonable functional model for the low-frequency vibrations described herein.

If the origin of the discrepancies between EIE_{obs} and EIE_{calc} is not calculational, then what experimental difficulties may have prevented a more accurate measure of the EIE_{obs}? The accuracy of the ND integrals in the assay of ^{2}H NMR spectra employed in the calculation of the [R_DD]/[**1**-ND-R_D] fraction was of concern. Integration of these resonances, often critical because of overlap in the R_D resonances of the hydrocarbon and organometallic components, proved to be difficult. Although we developed a consistent analytical procedure, the ND integrals may be low, resulting in an inflated [R_DD]/[**1**-ND-R_D] (or [**1**-R]/[**1**-ND-R′] in the intramolecular examples) ratio, and an artificially high EIE_{obs}. The greatest deviation in the intermolecular set is expected for the C_2H_6/C_2D_6 and $^cC_3H_6/^cC_3D_6$ cases, and some uncertainty in EIE_{obs} values for the $CH_2=CH_2/CD_2=CD_2$ and C_6H_6/C_6D_6 experiments may be inferred because integrals including the ND were utilized. In the intramolecular CH_xD_{4-x} ($x = 1-3$) examples, the deviation from calculated EIE scales with the importance of the ND integral in the three methane isotopologues, but ^{1}H NMR assays were used for the remaining intramolecular examples, which match much better with the observed EIEs. In summary, the −3 to +28% (($EIE_{obs} - EIE_{calc}$)/EIE_{obs}) deviations in observed vs calculated EIEs are mostly attributed to experimental difficulties, and the calculational models are sufficient to permit interpretation of the EIEs based on eq 4.

2. The MMI Term. The correspondence between the intermolecular EIE data and EIE_{calc} clearly substantiates inclusion and interpretation of the MMI term in evaluating intermolecular isotope effects. However, it will become apparent that the MMI term is attenuated by components of the EXC and EXP[−(ΔΔZPE/k_BT)] terms that derive from vibrations that are remnants of substrate free rotation and translation. Note that in the intramolecular cases, the MMI term is inconsequential because changes in the moments of inertia are trivial, and the masses of **1**-ND-R′ and **1**-R are the same.

3. Vibrational Analysis. For continuity, unscaled vibrational frequencies from the RHF/SBK(d) calculations were used for both **1′**-R and RH, and these appear as linear combinations of individual stretches, bends, and torsional vibrations. To interpret the EXC and ZPE terms for the intermolecular EIE_{calc} calculations, it was often expedient to correlate isotopically sensitive vibrations for each $(HO)_2(HNH)TiR_H$ (**1′**-R_H) with corresponding modes in the free hydrocarbon. Upon close inspection, and with the use of pictorial representations of the vibrations, all could be assigned on the basis of the major component individual modes, and a reasonable correlation between **1′**-R and RH was made when advantageous for discussion. The partitioning of the contributions to EXC and EXP[−(ΔΔZPE/k_BT)] in this fashion—while convenient in certain instances—presents a significant problem that should be kept in mind when reviewing the comments below. Due to the low symmetry, complexity, and varied deuteration of **1′**-R_H/**1′**-ND-R_D/**1′**-R/**1′**-ND-R′, the modes are mixed, and the extent of mixing is particularly problematic for low-energy vibrations. Consequently, when a vibration is assigned to a particular mode, that vibration typically contains varied contributions of other like-symmetry modes. As a corollary, the assigned mode may also contribute to a number of other like-symmetry vibrations.

Conventional descriptions of the substrate vibrations are indicated in Tables 3−5. In- and out-of-plane bends refer to motions with respect to the principal molecular planes of ethylene, benzene, and toluene, while perpendicular and parallel bends describe motions with respect to the C_3 ring in ^{c}PrH, or the C−C axis in ethane and the toluene Ph−CH_3; methane bends occur primarily within HCH planes. Frequencies relatively unrelated to the hydrocarbyl fragment are termed core vibrations, and remnants of rotational and translational movements pertaining to the free hydrocarbons are stated as such.

Isotopically sensitive vibrations in $(HO)_2(HNH)TiR_H$ (**1′**-R_H) include both the amide NH and the hydrocarbyl (R_H), whose vibrations correspond directly to those of the R_H of R_HH. The degree of mixing is different for R_HH and R_DD, and in some instances for **1′**-R_H versus R_HH; thus, all vibrations need to be scrutinized for their impact on EXC and EXP[−(ΔΔZPE/k_BT)] terms. Each **1′**-R_H has fewer isotopically sensitive hydrocarbyl-based vibrations than R_HH due to the loss of a C−H bond upon activation. The "missing" substrate vibrations can be correlated with a stretching vibration and in- or out-of-plane bending vibrations of an amide NH group, but it proved more informative to keep these contributions separate in subsequent discussions. Since an NH_2 was substituted for $NHSi^tBu_3$ in **1′**-R_H, NH vibrations of interest (i.e., the one that undergoes isotopic substitution) are mixed with those of the ancillary NH within symmetric and antisymmetric normal modes. These vibrations can be considered linear combinations of an isotopically sensitive NH mode and a nonisotopically sensitive mode, so both need to be analyzed to assess the influence of isotopic substitution on the EXC and EXP[−(ΔΔZPE/k_BT)] terms; they are combined and analyzed together in the discussions.

Although the majority of uncorrelated modes of $(HO)_2(HNH)TiR_H$ (**1′**-R_H) pertain to nonisotopically sensitive vibrations (e.g., Ti−O−H, N−Ti−O bends, etc.), some that involve motion of the hydrocarbyl fragment may be considered remnants of R_HH rotation and translation.[31] These vibrations are often decidedly mixed in composition, but in many cases a major component directly relates to a translation or rotation remnant. In Figure 2, the core vibrations of **1′**-CH_3 most closely resembling the rotations and translations of free methane, i.e., the "remnants", are illustrated. Similar sets of vibrational remnants can be found for the remaining **1′**-R, and a sampling of significant core vibrations of this type are given in Figure 3.

Most remnants are comprised primarily of carbon-framework motion, with little motion of the hydrogens relative to the carbons, and display only little to moderate changes in vibrational frequency upon isotopic substitution. In specific cases, a strong correlation between substrate rotation is observed, and these vibrations are strongly dependent on isotopic substitution. The situation arises when a rotation of the free hydrocarbon occurs about an axis which passes through all carbon atoms; the resulting "trapped" rotation in **1′**-R_H is then composed principally of hydrogen motion, with little carbon movement.

Table 3 exhibits the frequencies obtained for **1′**-CH_3, **1′**-ND-CD_3, CH_4, and CD_4 and shows each correlated and uncorrelated factor that contributes toward the EXC and EXP[−(ΔΔZPE/k_BT)] terms. Frequencies for the other **1′**-R_H, R_HH and pertinent isotopologues are available as Supporting Information. For the

(30) With Q defined as the product of the EXC and ZPE contributions, the Q's used in and calculated according to ref 28 were Q_{har}(**1**-CH_3) = 1.247, $Q_{fr\ rot}$(**1**-CH_3) = 3.714, Q_{hin}(**1**-CH_3) = 1.240, Q_{har}(**1**-ND-CH_3) = 1.760, $Q_{fr\ rot}$(**1**-ND-CH_3) = 5.250, Q_{hin}(**1**-ND-CH_3) = 1.750, Q_{har}(**1**-CH_3)/Q_{har}(**1**-ND-CD_3) = 0.7085, $Q_{fr\ rot}$(**1**-CH_3)/$Q_{fr\ rot}$(**1**-ND-CD_3) = 0.7074, Q_{har}(**1**-CH_3)/Q_{har}(**1**-ND-CD_3) = 0.7086.

(31) In an analysis of CH_4 vs CD_4 binding to $Os(CO)_4$, Bender recognized that contributions to EXC and EXP[−(ΔΔZPE)] terms by rotational and translational remnants effectively attenuated the MMI term. Bender, B. R., personal communication. Analysis based on computational models by: Avdeev, V. I.; Zhidomirov, G. M. *Catal. Today* **1998**, *42*, 247−261.

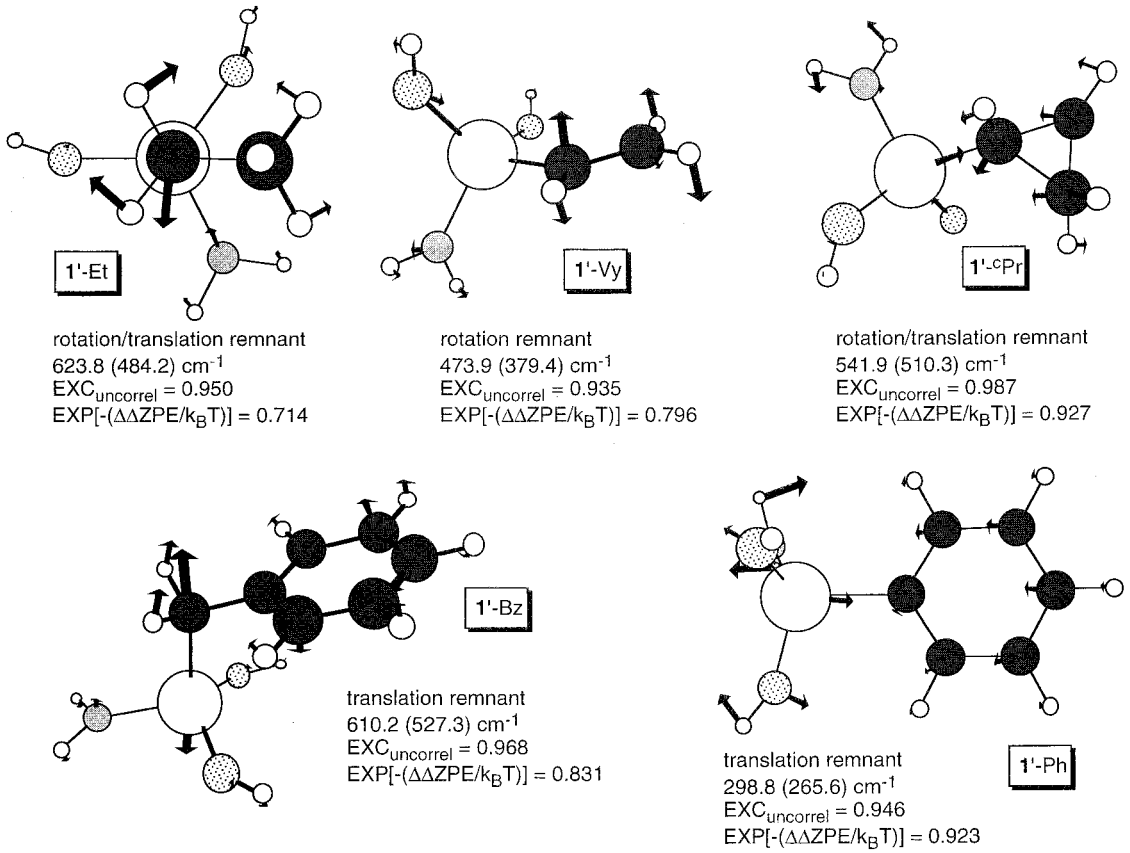

Figure 3. Some core vibrational remnants of RH rotation and translation in **1′**-RH (**1′**-ND-RD) and their uncorrelated contributions to EXC and EXP[$-(\Delta\Delta ZPE/k_BT)$].

remainder of the text, *no further frequencies will be tabulated*; the calculations will be discussed in terms of correlated and uncorrelated EXC and EXP[$-(\Delta\Delta ZPE/k_BT)$] contributions as defined below.

4. The EXC Term. Since the individual $(1 - \exp(-h\nu_i/k_BT))^{-1}$ factors which constitute the EXC term commute, the contribution to EIE_{calc} from EXC may be calculated from eq 6 in a manner convenient for interpretation. Tables 3 and 4 contain two types of entries: contributions to the EXC term given for vibrations correlated between **1**-R_H and R_HH (eq 20), and uncorrelated contributions to the EXC term (eqs 21 and 22).

$$\frac{(1 - \exp(-h\nu_i^{\mathbf{1}'-(ND)-R_D}/k_BT))(1 - \exp(-h\nu_i^{R_HH}/k_BT))}{(1 - \exp(-h\nu_i^{\mathbf{1}'-R_H}/k_BT))(1 - \exp(-h\nu_i^{R_DD}/k_BT))} = \mathrm{EXC}_{\text{correl contrib}} \quad (20)$$

$$\frac{(1 - \exp(-h\nu_i^{\mathbf{1}'-(ND)-R_D}/k_BT))}{(1 - \exp(-h\nu_i^{\mathbf{1}'-R_H}/k_BT))} = \mathrm{EXC}_{\text{uncorrel contrib}} \quad (21)$$

$$\frac{(1 - \exp(-h\nu_i^{R_HH}/k_BT))}{(1 - \exp(-h\nu_i^{R_DD}/k_BT))} = \mathrm{EXC}_{\text{uncorrel contrib}} \quad (22)$$

$$\frac{(1 - \exp(-h\nu_i^{\mathbf{1}'-(ND)-R'}/k_BT))}{(1 - \exp(-h\nu_i^{\mathbf{1}'-R}/k_BT))} = \mathrm{EXC}_{\text{contrib}} \quad \text{(intramolecular)} \quad (23)$$

Factoring the EXC into contributions from correlated and individual modes provides some insight toward unraveling the origins of the EIE. Note that lower frequency vibrations contribute greatly to the EXC term. Individual contributions are exemplified in Table 3, while in Table 4, the vibrations are grouped further into products of related $EXC_{correl\ contrib}$, products of similar $EXC_{uncorrel\ contrib}$, and products of the intramolecular equivalents (eq 23).

As eq 21 reveals for intermolecular cases, the contribution from an individual mode in the complex will always favor the deuterated molecule because of its lower frequency; hence an inverse factor will result. Equation 20 shows that deuterated species are in both the numerator and denominator, but with one exception (vide infra) none of the correlated factors are greater than 1.02, because modes in **1′**-(ND)-R_D/**1′**-R_H are generally lower than their counterparts in R_HH/R_DD. In the intramolecular cases (eq 23), the majority of important EXC contributions to EIE_{calc} are inverse because a number of low-frequency torsions involving the amide functionality favor the ND derivative. Other modes besides NH bends—especially the remnants—are less important in intramolecular EIEs than in intermolecular EIEs because of the relatively even distribution of deuterium.

In summary, in accord with the assignments and method of analysis discussed above, the critical contributions to the EXC product encompass those vibrations with an NH component, and low-frequency core vibrations that contain minor to moderate components resembling rotations and translations of the free substrate.

4. The EXP[$-(\Delta\Delta ZPE/k_BT)$] Term. The same breakdown of frequencies into correlated and uncorrelated contributions to EXP[$-(\Delta\Delta ZPE/k_BT)$] was used in Table 3 according to eqs 24−27.

Table 3. Vibrational Frequencies,[a] EXC, and EXP[$-(\Delta\Delta ZPE/k_BT)$] Terms for **1′**-ND-CD$_3$ + CH$_4$ ⇄ **1′**-CH$_3$ + CD$_4$

assigned mode[b]	**1′**-CH$_3$	**1′**-ND-CD$_3$	substr sym or remnant[c]	CH$_4$	CD$_4$	EXC$_{contrib}$[d]	EXP[$-(\Delta\Delta ZPE/k_BT)$]$_{contrib}$[e]
			Correlated CH Stretches[f]				
CH str	3133.4	2248.1	a_1	3154.7	2231.6	1.000	1.096
	3225.1	2387.8	t_1	3291.2	2440.2	1.000	1.034
	3239.5	2399.4	t_1	3291.2	2440.3	1.000	1.026
			Uncorrelated CH and NH Stretches[g]				
			t_1	3291.2	2440.3	1.000	7.809
NH sym str	3699.5	2734.5				1.000	0.0972
NH antisym str	3793.9	3749.0				1.000	0.8972
			Correlated Bends[f]				
CH in-plane	1544.1	1119.2	e	1659.2	1173.7	0.999	1.158
CH in-plane	1543.6	1118.9	e	1659.2	1173.7	0.999	1.158
CH out-of-plane	1319.6	1038.9	t_2	1439.5	1086.7	0.999	1.190
			Uncorrelated CH and NH Bends[g]				
			t_2	1439.5	1086.7	1.004	2.344
			t_2	1439.5	1086.7	1.004	2.344
NH sym in-plane	1656.4	1467.9				1.000	0.634
NH antisym in-plane	578.9	492.2				0.966	0.811
NH sym out-of-plane	426.0	392.4				0.974	0.922
NH antisym out-of-plane	304.4	256.9				0.923	0.892
			Other Uncorrelated (Core, Remnant)[g]				
OH str	4188.1	4188.1				1.000	1.000
OH str	4184.2	4184.2				1.000	1.000
TiO str	843.9	832.9				0.999	0.974
TiO, TiN str	803.2	789.1				0.999	0.967
TiO, TiN str	717.6	705.3				0.998	0.971
Me torsion	657.0	515.4	*x* rot.			0.957	0.710
Me torsion	647.1	510.2	*y* rot.			0.957	0.719
TiC stretch	579.9	536.0	*z* trans.			0.985	0.899
OTiO, TiOH bend	293.9	293.3				0.999	0.999
NTiOH torsion	240.3	229.0				0.974	0.973
OTiN, OTiC bend	200.3	186.0	*x* trans.			0.956	0.966
NTiC wag	190.8	177.1	*y* trans.			0.955	0.968
OTiN, OTiC bend	170.3	154.9	rot.			0.940	0.964
OTiO, TiOH bend	167.4	163.2				0.983	0.990
Me torsion	161.7	116.0	*z* rot.			0.791	0.896
NTiO, TiOH bend	123.1	121.8				0.992	0.997
CTiOH torsion	103.5	102.6				0.993	0.998
CTiOH torsion	64.1	63.7				0.995	0.999

[a] Representative of all **1′**-R, these unscaled frequencies are taken directly from calculations of **1′**-CH$_3$, **1′**-ND-CD$_3$, CH$_4$, and CD$_4$ at 24.8 °C. [b] Modes were assigned by viewing each vibration and assessing its major component. [c] Symmetry of the substrate mode or assigned vibrational remnant. [d] Product of EXC$_{contrib}$ = 0.500. [e] Product of EXP[$-(\Delta\Delta ZPE/k_BT)$]$_{contrib}$ = 0.949. [f] Correlated EXC contributions contain factors from both the metal complex and substrate according to eq 20. Correlated EXP[$-(\Delta\Delta ZPE/k_BT)$] contributions contain factors from both the metal complex and substrate according to eq 24. [g] Uncorrelated contributions are simply derived from **1′**-CH$_3$ and **1′**-ND-CD$_3$ (EXC, eq 21; EXP[$-(\Delta\Delta ZPE/k_BT)$], eq 25), or R$_H$H and R$_D$D (eq 22, eq 26).

$$\exp(-h\nu_i^{\mathbf{1}'-R_H}/2k_BT)\exp(h\nu_i^{\mathbf{1}'-(ND)-R_D}/2k_BT)\exp(-h\nu_i^{R_DD}/2k_BT)\exp(h\nu_i^{R_HH}/2k_BT) = \mathrm{EXP}[-(\Delta\Delta ZPE/k_BT)]_{correl\ contrib} \quad (24)$$

$$\exp(-h\nu_i^{\mathbf{1}'-R_H}/2k_BT)\exp(h\nu_i^{\mathbf{1}'-(ND)-R_D}/2k_BT) = \mathrm{EXP}[-(\Delta\Delta ZPE/k_BT)]_{uncorrel\ contrib} \quad (25)$$

$$\exp(-h\nu_i^{R_DD}/2k_BT)\exp(h\nu_i^{R_HH}/2k_BT) = \mathrm{EXP}[-(\Delta\Delta ZPE/k_BT)]_{uncorrel\ contrib} \quad (26)$$

$$\exp(-h\nu_i^{\mathbf{1}'-R}/2k_BT)\exp(h\nu_i^{\mathbf{1}'-(ND)-R'}/2k_BT) = \mathrm{EXP}[-(\Delta\Delta ZPE/k_BT)]_{contrib}\ \ (intramolecular) \quad (27)$$

In the intramolecular cases, correlations between reactant **1′**-ND-R′ and product **1′**-R are relatively easily determined, and the EXP[$-(\Delta\Delta ZPE/k_BT)$]$_{contrib}$ for each vibration is shown in eq 27. Again, products of related contributions are conveniently grouped in Table 5. As the exponential form of the ZPE contribution indicates, the term will favor the deuterated species over the protiated, but the strongest vibrations are not necessarily the most influential because of differences in degrees of mode mixing.

Uncorrelated ZPE contributions to the intermolecular EIE$_{calc}$ pertinent to the metal complex are always inverse, since **1′**-(ND)-R$_D$ lies on the reactant side and **1′**-R$_H$ on the product side in Scheme 1. In opposition, uncorrelated contributions from related modes of the hydrocarbon are always normal, since R$_D$D is the product. In the correlated contributions, both normal and inverse effects are apparent, with the majority being normal due to typically stronger modes of R$_H$H/R$_D$D relative to their counterparts in **1′**-R$_H$/**1′**-(ND)-R$_D$D.

Vibrations having significant impact on the EXP[$-(\Delta\Delta ZPE/k_BT)$] product are uncorrelated NH stretches and bends that afford inverse contributions, uncorrelated CH stretches, correlated and uncorrelated CH bending vibrations, and low-frequency core vibrations containing minor to moderate remnants of substrate rotations and translations that lead to substantial inverse terms.

Intermolecular EIE Specifics. 1. MMI and Remnants. Before an assessment of the EIEs can begin, the MMI term, and the vibrational remnants of hydrocarbon free rotation and

Table 4. EXC Terms for Inter- and Intramolecular EIEs Factored According to Vibrational Type

	stretches			in-plane/perpendicular bends[a]			out-of-plane/parallel bends[a]						
1′-R_H/**1′**-*R*	CH[b]	CH[c]	NH[d]	CH[b]	CH[c]	NH[d]	CH[b]	CH[c]	NH[d]	internal rot.[e]	CC[b]	rem[f]	product[g]
Intermolecular: **1′**-ND-R_D + R_HH ⇄ **1′**-R_H + R_DD													
1′-CH_3	1.000	1.000	1.000	0.998	1.004	0.966	0.999	1.004	0.899			0.572	0.500
1′-C_2H_5	1.000	1.000	1.000	0.999	1.003	0.969	1.024	1.001	0.853	1.019	1.002	0.635	0.551
1′-$^cC_3H_5$	1.000	1.000	1.000	1.014	1.003	0.962	1.032	1.004	0.923		1.012	0.649	0.616
1′-HC═CH_2	1.000	1.000	1.000	1.018	1.005	0.969	1.003	1.016	0.921		1.000	0.635	0.591
1′-C_6H_5	1.000	1.000	1.000	1.002	1.010	0.970	1.006	1.018	0.926		1.028	0.735	0.702
1′-C_7H_7	1.000	1.000	1.000	0.999	1.006	0.963	1.002	1.008	0.868	1.302	1.057	0.704	0.822
2′-H_2CCH_2	1.000			1.012			1.028				0.990[h]	0.746	0.767
Intramolecular: **1′**-ND-R′ ⇄ **1′**-R (RH = R′D)[i–k]													
1′-CH_2D	1.000		1.000	1.002		0.968			0.907			1.083	0.956
1′-CHD_2	1.000		1.000	1.005		0.967			0.909			1.057	0.934
1′-CD_3	1.000		1.000	1.006		0.967			0.906			1.050	0.925
1′-CH_2CD_3	1.000		1.000	1.003		0.966	0.996		0.865	1.085	1.002	1.066	0.969
1′-$^cC_3H_3D_2$	1.000		1.000	0.986		0.964	1.025		0.941		1.012	0.935	0.869
1′-DC═CDH	1.000		1.000	1.012		0.969	1.012		0.917		1.000	1.025	0.931
1′-$C_6H_2D_3$	1.000		1.000	0.998		0.969	1.025		0.932		1.009	0.921	0.855
1′-CHDPh	1.000		1.000	1.001		0.964	1.008		0.875	1.038	1.046	0.942	0.871

[a] Bends relative to C−C axes or ring planes where appropriate. [b] Products of correlated (eq 20) terms, except for unique CC factors (e.g., the only C−C stretch in **1′**-C_2H_5) represented by an individual correlated (eq 20) term. [c] Single, uncorrelated (eq 22) hydrocarbon term. [d] Product of uncorrelated (eq 21) sym NH and antisym NH terms (see text). [e] Correlated (eq 20) term. [f] Product of uncorrelated (eq 21) terms. Where possible, rot. and trans. remnants have been located among the core vibrations (see text), but these modes are widely distributed, and are factored together with other core vibrations. [g] Product of all terms. [h] Product of a correlated (symmetric) and uncorrelated (unsymmetric) term. [i] Intramolecular CH, CC and remnant terms are products of intramolecular contributions (eq 23), except for unique CC factors (e.g., the only C−C stretch in **1′**-CH_2CD_3) represented by an individual correlated (eq 20) term. [j] Intramolecular NH factors are products of sym NH and antisym NH terms (eq 23). [k] Internal rotations are represented by an individual correlated (eq 20) term.

Table 5. EXP[−(ΔΔZPE/k_BT)] Terms for Inter- and Intramolecular EIEs factored According to Vibrational Type

	stretches			in-plane/perpendicular bends[a]			out-of-plane/parallel bends[a]						
1′-R_H/**1′**-R	CH[b]	CH[c]	NH[d]	CH[b]	CH[c]	NH[d]	CH[b]	CH[c]	NH[d]	internal rot.[e]	CC[b]	rem[f]	product[g]
Intermolecular: **1′**-ND-R_D + R_HH ⇄ **1′**-R_H + R_DD													
1′-CH_3	1.163	7.809	0.0872	1.596	2.345	0.5143		2.345	0.8222			0.323	0.950
1′-C_2H_5	1.141	7.714	0.0872	1.097	2.910	0.5237	1.094	1.871	0.7698	1.096	1.045	0.561	1.299
1′-$^cC_3H_5$	1.139	7.751	0.0874	0.929	2.601	0.5049	1.012	1.466	0.8568		1.332	0.737	1.177
1′-HC═CH_2	1.132	7.933	0.0872	0.882	2.607	0.5264	0.974	1.851	0.8651		1.133	0.552	0.924
1′-C_6H_5	1.019	8.204	0.0872	1.013	2.265	0.5217	0.983	1.669	0.8549		1.215	0.807	1.200
1′-C_7H_7	1.086	6.513	0.1058	0.966	2.765	0.5500	1.576	1.497	0.8024	0.771	1.040	0.743	1.240
2′-H_2CCH_2	1.236			1.375			0.744				0.850[h]	0.442	0.476
Intramolecular: **1′**-ND-R′ ⇄ **1′**-R (RH = R′D)[i–k]													
1′-CH_2D	7.797		0.0872		2.263	0.5211			0.8365			1.356	0.908
1′-CHD_2	7.992		0.0872		2.475	0.5178			0.8456			1.288	0.976
1′-CD_3	7.806		0.0872		2.730	0.5184			0.8372			1.215	0.982
1′-CH_2CD_3	8.393		0.0872		3.417	0.5180		1.512	0.7865	1.084	1.173	0.759	1.482
1′-$^cC_3H_3D_2$	8.546		0.0874		0.990	0.5123		1.980	0.8815		2.401	0.918	1.457
1′-DC═CDH	8.023		0.0872		2.195	0.5238		1.697	0.8235		1.034	0.925	1.075
1′-$C_6H_2D_3$	8.208		0.0872		1.292	0.5219		1.885	0.8692		2.013	0.918	1.460
1′-CHDPh	6.616		0.1058		1.425	0.5505		1.627	0.8160	1.300	1.271	0.942	1.134

[a] Bends relative to C−C axes or ring planes where appropriate. [b] Products of correlated (eq 24) terms, except for unique CC factors (e.g., the only C−C stretch in **1′**-C_2H_5) represented by an individual correlated (eq 24) term. [c] Single, uncorrelated (eq 26) hydrocarbon term. [d] Product of uncorrelated (eq 25) sym NH and antisym NH terms (see text). [e] Correlated (eq 24) term. [f] Product of uncorrelated (eq 25) terms. Where possible, rot. and trans. remnants have been located among the core vibrations (see text), but these modes are widely distributed, and are factored together with other core vibrations. [g] Product of all terms. [h] Product of a correlated (symmetric) and uncorrelated (unsymmetric) term. [i] Intramolecular CH, CC, and remnant terms are products of intramolecular contributions (eq 23), except for unique CC factors (e.g., the only C−C stretch in **1′**-CH_2CD_3) represented by an individual correlated (eq 20) term. [j] Intramolecular NH factors are products of sym NH and antisym NH terms (eq 23). [k] Internal rotations are represented by an individual correlated (eq 20) term.

translation present in the various isotopologues of **1′**-R, need to be addressed. In Table 6, the symmetry-corrected EIE_{calc} values are presented, but their components are reassessed as follows. Each MMI term is multiplied by the two terms that comprise the vibrational remnants: the product of the various core and remnant $EXC_{uncorrel}$ terms (eq 21), and the product of the corresponding $EXP[-(\Delta\Delta ZPE/k_BT)]_{uncorrel}$ terms (eq 25). The resulting attenuated MMI expression, termed AMMI, essentially encompasses the distribution of the free energy associated with rotation and translation of the free hydrocarbon and its bound equivalent in **1′**-R_H. Note that this term is actually inverse; i.e., the vibrational remnants of rotation and translation effectively cancel the MMI contribution[31]—in fact, they overcompensate for it. There are two ways in which to proceed with the analysis. The AMMI term can be minutely analyzed for differences in response to changes in R, but remember that the breakdown of the vibrational frequencies was somewhat subjective, and it is very likely the mode mixing is greater for the **1′**-ND-R_D species in comparison to **1′**-R_H, providing a rationale for the inverse AMMI. Given the latter caveat, a safer analysis assumes that the AMMI term is essentially ∼1 for each case.

2. EXC and Corrections. The next heading in Table 6 gives the remainder of the EXC term for each case, once the remnant contributions have been divided out (EXC/EXC_{rem}). From Table

Table 6. Calculated Intermolecular and Intramolecular Isotope Effects Redistributed with Attenuated MMI (AMMI)[a,b]

R_H/R_D (inter) or RH (intra)	EIE_{calc}/SYM	AMMI = MMI × EXC_{rem} × $EXP[-(\Delta\Delta ZPE/k_BT)]_{rem}$	EXC/EXC_{rem}	$EXP[-(\Delta\Delta ZPE/k_BT)]/EXP[-(\Delta\Delta ZPE/k_BT)]_{rem}$
		Intermolecular		
CH_4/CD_4	1.88	0.730	0.874	2.941
C_2H_6/C_2D_6	1.93	0.958	0.868	2.316
$^cC_3H_6/^cC_3D_6$	1.48	0.976	0.949	1.597
$H_2C=CH_2/D_2C=CD_2$	1.34	0.859	0.931	1.674
C_6H_6/C_6D_6	1.26	0.884	0.955	1.487
C_7H_8/C_7D_8	1.55	0.795	1.168	1.669
$-H_2CCH_2-/-D_2CCD_2-$	0.893	0.823	1.009	1.077
		Intramolecular		
CDH_3	0.87	1.469	0.883	0.670
CD_2H_2	0.91	1.361	0.884	0.758
CD_3H	0.91	1.276	0.881	0.808
CD_3CH_3	1.44	0.809	0.909	1.953
1,1-$^cC_3H_4D_2$	1.27	0.858	0.929	1.587
trans-HDC=CHD	1.00	0.948	0.908	1.162
1,3,5-$C_6H_3D_3$	1.25	0.846	0.928	1.590
$PhCH_2D$	0.99	0.887	0.920	1.204

[a] EXC_{rem} refers to core vib. and rot., trans. remnant contributions in Tables 3 and 4. [b] $EXP[-(\Delta\Delta ZPE/k_BT)]_{rem}$ refers to core vib. and rot., trans. remnant contributions in Tables 3 and 5.

4 it can be seen that the major remaining contributors to the EXC term are the bending vibrations involving the NH, but the EXC/EXC_{rem} values are all within 10% of one another with the exception of the toluene case. The unusual low-frequency methyl rotor of toluene, essentially a free rotor (41.4 cm^{-1}, 29.7 cm^{-1} in C_7D_7), becomes substantially hindered (669.9 cm^{-1}, 541.5 cm^{-1} in **1′**-$CD_2C_6D_5$) in **1′**-CH_2Ph, causing a large 1.302 $EXC_{correl\ contrib}$ that renders the EXC term of the toluene case comparatively large. Given the comments above, especially those regarding mode mixing, it is difficult to rationalize a discussion regarding the impact on EIE by EXC/EXC_{rem} values, given their rather meager differences.

3. EXP[−(ΔΔZPE/k_BT)] and Corrections. When the remnant contributions are removed from the $EXP[-(\Delta\Delta ZPE/k_BT)]$ term, the $EXP[-(\Delta\Delta ZPE/k_BT)]/EXP[-(\Delta\Delta ZPE/k_BT)]_{rem}$ version reveals the expected major differences in contributions as a function of −R. It should, because the fundamental bond exchange—R_HH vs NH and R_DD vs ND—requires the breaking and making of distinctly different bonds. Since section 1 above argues for AMMI ∼1, where should the corrections to the AMMI column of Table 6 be applied? Since EXC/EXC_{rem} is expressing little or no response to changes in −R, the AMMI correction should be applied to $EXP[-(\Delta\Delta ZPE/k_BT)]/EXP[-(\Delta\Delta ZPE/k_BT)]_{rem}$. Note that multiplication of the AMMI and $EXP[-(\Delta\Delta ZPE/k_BT)]/EXP[-(\Delta\Delta ZPE/k_BT)]_{rem}$ columns affords values that parallel the EIE_{calc}/SYM numbers—as they must—and adds some credence to the above assumptions.

4. Intermolecular EIEs. The EIE_{obs} and EIE_{calc} values are reasonably consistent, especially considering the aforementioned analytical problems, and vary from 1.22(7) for the C_6H_6/C_6D_6 case to 2.22(8) for the ethane/ethane-d_6 example (Table 2). On the basis of the arguments presented above, the differences in the EIEs as a function of R need to be discussed in view of zero-point energy contributions. Table 5 shows that correlated stretching vibrations do not distinguish between variations in R. The correlated CH stretching contributions to $EXP[-(\Delta\Delta ZPE/k_BT)]$ are slightly >1, presumably because the replacement of an −H by $-Ti(OH)_2(NH_2)$ slightly lowers the frequencies of the hydrocarbyl piece of the organometallic relative to the free hydrocarbon. The products of the CH and NH stretching contributions for all intermolecular cases involving **1′**-R_H are within 8.6% of each other—within 5.9% if either "extreme" case, **1′**-C_6H_5 (0.729) or **1′**-CH_3 (0.792), is excluded—and their subtle deviations do not correlate with EIE. Examination of the uncorrelated NH stretching combinations reveals little change in $\exp(-h\nu_{NH}^{1'-R_H}/2k_BT)\ \exp(h\nu_{ND}^{1'-(ND)-R_D}/2k_BT)$ factors as a function of R (R ≠ CH_2Ph), and the only significant variation in the $\exp(-h\nu_{CD}^{R_DD}/2k_BT)\ \exp(h\nu_{CH}^{R_HH}/2k_BT)$ component is due to R = CH_2Ph. This is simply because T = 50.0 °C rather than 24.8 °C, and it is offset by the NH stretching factors. The products of the CH and NH stretching contributions are inverse, since the amide NH(D) is in a more strongly bound position—in terms of force constants—relative to a CH(D) in $R_HH(R_DD)$.

The remaining contributions from bending modes—both in-plane or perpendicular and out-of-plane or parallel—provide the greatest impact on the EIE. Some additional contributions are derived from carbon-based vibrations that are subtly mixed to varying degrees with CH/D modes; the cyclopropyl and phenyl cases exhibit fairly large, normal contributions due to carbon-based vibrations. By examining the components of the uncorrelated NH vibrations (Figure 4), it can be seen that bending contributions are dominated by the modes of the R_DD products vs the R_HH reactants. Figure 5 illustrates each substrate and its critical bending modes that "disappear", i.e., become NH-based, upon activation. The product of the $\exp(-h\nu_{NH}^{1'-R_H}/2k_BT)\ \exp(h\nu_{ND}^{1'-(ND)-R_D}/2k_BT)$ factors (sym and unsym, eq 25) that refers to the in-plane vibration and the $\exp(-h\nu_{NH}^{1'-R_H}/2k_BT)\ \exp(h\nu_{ND}^{1'-(ND)-R_D}/2k_BT)$ factors (sym and unsym, eq 25) that refers to the out-of-plane vibration gives the uncorrelated contribution to the $EXP[-(\Delta\Delta ZPE/k_BT)]$ term from NH bends. The products are essentially the same (i.e., 0.403 (**1′**-Et case), 0.423 (**1′**-Me), 0.433 (**1′**-^{c}Pr), 0.443 (**1′**-Bz), 0.446 (**1′**-C_6H_5), and 0.455 (**1′**-$CHCH_2$)) for every intermolecular case, because the actual NH bending frequencies are basically independent of R.

The uncorrelated $\exp(-h\nu_{CD}^{R_DD}/2k_BT)\ \exp(h\nu_{CH}^{R_HH}/2k_BT)$ terms of eq 26 vary substantially, and in concert with correlated CH bends (Figure 6) and carbon-based vibrations (e.g., eq 24) comprise the basis of discrimination in EIEs as a function of −R. Using these modes (Figure 5), one arrives at relative ranking based on CH contributions to $EXP[-(\Delta\Delta ZPE/k_BT)]$ of **1′**-Me > **1′**-Et > **1′**-Bz > **1′**-cPr ≥ **1′**-$CHCH_2$ ≥ **1′**-C_6H_5, which essentially mirrors the calculated EIEs except for the transposition of **1′**-Me and **1′**-Et. The latter is probably due to the mode mixing problem, because application of AMMI to these products reverses their order. While it would be convenient to point to a single type of vibration and gain the requisite understanding of the EIEs on the basis of $EXP[-(\Delta\Delta ZPE/k_BT)]$ contributions, such a simple answer was not forthcoming, and a brief

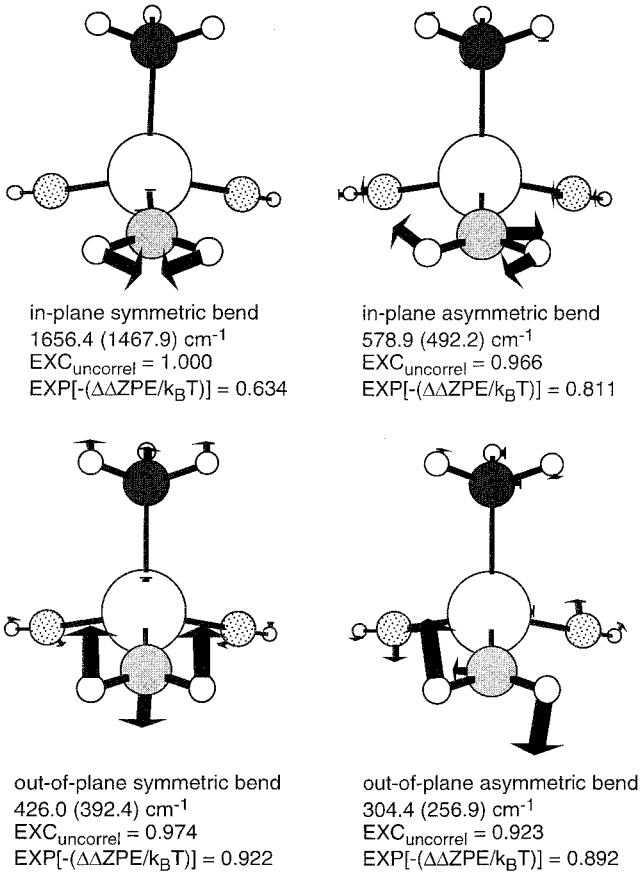

Figure 4. NH_2 symmetric and asymmetric bends of **1′**-CH_3 (**1′**-ND-CD_3) and their uncorrelated contributions to EXC and EXP[$-(\Delta\Delta ZPE/k_BT)$]. Related vibrations and contributions to EIEs of the remaining **1′**-R_H (**1′**-ND-R_D) are similar.

discussion of each case will be undertaken. In each, only those CH factors that help distinguish the various cases are given.

a. 1′-(ND)-CD_3 + CH_4 ⇄ 1′-CH_3 + CD_4. The exp$(-h\nu_{CD}^{R_DD}/2k_BT)$ exp$(-\nu_{CH}^{R_HH}/2k_BT)$ terms of eq 26 corresponding to uncorrelated t_2 bending modes of CH_4/CD_4 each provide a 2.345 contribution (Figure 5), and another 1.596 is provided by the correlated CH vibrations (eq 24). These three terms contribute 8.774 toward the EXP[$-(\Delta\Delta ZPE/k_BT)$] term.

b. 1′-(ND)-C_2D_5 + C_2H_6 ⇄ 1′-C_2H_5 + C_2D_6. Correlated CH bending vibrations only afford factors of 1.098 and 1.094 (however, within this product a single correlated vibration comprised mostly of CCH bending contributes 1.258 due to a decrease in the frequency of this a_{2u} "double umbrella" bending mode of ethane (1496.3 cm^{-1}) upon perdeuteration (1143.4 cm^{-1}); see Figure 6). In contrast, the exp$(-h\nu_{CD}^{R_DD}/2k_BT)$ exp$(h\nu_{CH}^{R_HH}/2k_BT)$ terms of eq 26 corresponding to the perpendicular and parallel bending modes of the substrate generate 2.910 and 1.871 factors (Figure 5), respectively. These are augmented by correlated terms from a single internal rotation (1.096) and the C−C stretch (1.045). The product of all of these factors contributes 7.492 toward the EXP[$-(\Delta\Delta ZPE/k_BT)$] term.

c. 1′-(ND)-$^cC_3D_5$ + $^cC_3H_6$ ⇄ 1′-$^cC_3H_5$ + $^cC_3D_6$. The exp$(-h\nu_{CD}^{R_DD}/2k_BT)$ exp $(h\nu_{CH}^{R_HH}/2k_BT)$ terms of eq 26 corresponding to perpendicular and parallel bending modes of the $^cC_3H_6$ vs $^cC_3D_6$ generate factors of 2.601 and 1.466 (Figure 5), respectively. A moderately inverse contribution (0.929; see Figure 6) from correlated in-plane bends is counteracted by a small out-of-plane bending correlated contribution of 1.012 and some correlated, carbon-based ring-breathing and -stretching modes that contribute a product of 1.332. These features contribute 4.775 toward the EXP[$-(\Delta\Delta ZPE/k_BT)$] term.

d. 1′-(ND)-$CD{=}CD_2$ + C_2H_4 ⇄ 1′-$CH{=}CH_2$ + C_2D_4. Contributions of 2.607 and 1.851 from the exp$(-h\nu_{CD}^{R_DD}/2k_BT)$ exp$(h\nu_{CH}^{R_HH}/2k_BT)$ terms of eq 26 corresponding to in-plane and out-of-plane bending modes of the $H_2C{=}CH_2$ vs $D_2C{=}CD_2$ (Figure 5), respectively, are counteracted by inverse contributions from correlated CH in-plane (0.882; see Figure 6) and out-of-plane (0.974) bending vibrations. The C=C stretch also provides a factor of 1.133, leading to a 4.697 contribution toward the EXP[$-(\Delta\Delta ZPE/k_BT)$] term by these products.

e. 1′-ND-C_6D_5 + C_6H_6 ⇄ 1′-C_6H_5 + C_6D_6. Factors of 2.265 and 1.669 arise from the exp$(-h\nu_{CD}^{R_DD}/2k_BT)$ exp$(h\nu_{CH}^{R_HH}/2k_BT)$ terms of eq 26 corresponding to in-plane and out-of-plane bending modes of the C_6H_6 vs C_6D_6 (Figure 5), respectively. Other correlated CH in-plane (1.013) and out-of-plane (0.983) bending vibrations contribute minimally, but the product of correlated ring-stretching and breathing modes provides a factor of 1.215, leading to a contribution of 4.573 toward the EXP [$-(\Delta\Delta ZPE/k_BT)$] term by these products.

f. 1′-ND-$CD_2C_6D_5$ + C_7H_8 ⇄ 1′-$CH_2C_6H_5$ + C_7D_8; 50.0 °C. The exp$(-h\nu_{CD}^{R_DD}/2k_BT)$ exp$(h\nu_{CH}^{R_HH}/2k_BT)$ terms of eq 26 corresponding to perpendicular and parallel bending modes of the C_7H_8 vs C_7D_8 (Figure 5) provide factors of 2.765 and 1.497 (50.0 °C), respectively. Correlated CH bending vibrations due to the Ph ring are relatively inconsequential, with the in-plane (0.949) effectively canceling out the out-of-plane (1.062) contributions, but vibrations associated with the CH_2 unit afford significant factors. While the correlated in-plane vibration amounts to 1.018, the out-of-plane contribution is 1.484 because a large normal contribution (1.604; see Figure 6) occurs from a CH_2 bend (1197.8 (997.2) cm^{-1}) parallel to the Ti−C−C plane that correlates with the much higher frequency methyl "umbrella" vibration of toluene (1531.5 (1118.5) cm^{-1}). The aforementioned internal rotor provides an inverse contribution (0.771; see Figure 6) that is partially offset by various carbon-based modes (1.040). All of these products contribute 5.014 toward the EXP[$-(\Delta\Delta ZPE/k_BRT)$] term.

5. A Special Case: 2′-C_2D_4 + C_2H_4 ⇄ 2′-C_2H_4 + C_2D_4. EXP[$-(\Delta\Delta ZPE/k_BT)$] contributions from correlated stretching vibrations in the intermolecular EIE_{calc} pertaining to metallacycle **2′**-C_2H_4 arise from a decrease in vibrational frequencies that reflect the sp^2-to-sp^3 hybridization change of the C_2H_4 fragment.[32] Though the a_{1g}-type stretching combination contributes a mildly inverse ZPE factor of 0.948, the other three stretching modes produce normal contributions, giving a product ZPE factor of 1.235 for all CH stretches.

This particular case proved the most difficult to correlate, perhaps because the dramatic drop in symmetry from D_{2h} (ethylene) to C_s (**2′**-C_2H_4) permits a large degree of mixing among the bending modes. The in-plane bending vibrations contribute a substantial normal factor of 1.375 due mostly to a mode correlating with the a_{1g} ethylene bend (1.320). This is counteracted by out-of-plane bending vibrations that display an inverse contribution (0.744) attributable to the higher frequencies of these vibrations in **2′**-C_2H_4 relative to free ethylene. Realistically, the variation between in- and out-of-plane contributions may be better construed as arising from difficulties in correlating modes within such different symmetries. Inverse factors of 0.861 and 0.799 are obtained from the a_u and b_{1u} (Figure 7) combinations, and a slightly normal factor of 1.081 from the b_{2g} combination. The b_{1u} mode is the out-of plane deformation

(32) Streitweiser, A.; Jagow, R. H.; Fehey, R. C.; Suzuki, S. *J. Am. Chem. Soc.* **1958**, *80*, 2326−2332.

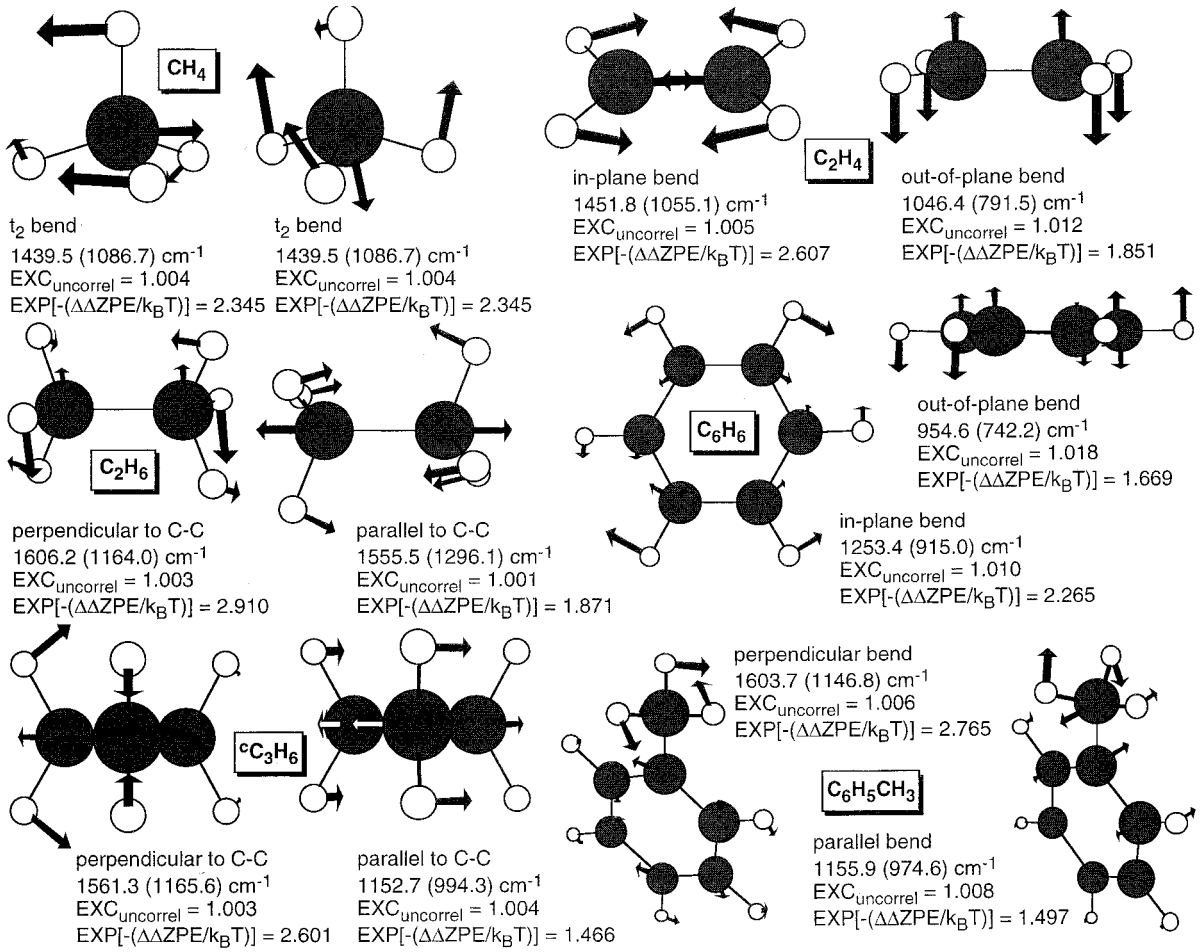

Figure 5. Uncorrelated R_HH (R_DD) vibrations and their contributions to EXC and EXP[$-(\Delta\Delta ZPE/k_BT)$].

originally implicated by Streitwieser et al. as the primary cause of inverse secondary kinetic isotope effects in reactions involving sp^2-to-sp^3 hybridization changes.[32]

In this EIE$_{calc}$, the carbon−carbon stretching vibration also manifests a significant inverse contribution (0.850) as a result of the decrease in carbon−carbon bond strength and hence a stretching frequency upon loss of the π-bond on going from ethylene (1835.3 (1699.4) cm^{-1}) to **2′**-C_2H_4. The EXP [$-(\Delta\Delta ZPE/k_BT)$] contribution for this correlated vibration is computed as a product of three terms because the carbon−carbon stretch is split into two normal modes (1031.5 (950.3) cm^{-1}; 975.0 (852.8) cm^{-1}) in **2′**-C_2H_4 due to mixing with the carbon−nitrogen stretch.

As stressed above, core vibrations, including those that appear as remnants of free ethylene rotation and translation, essentially compensate (EXP[$-(\Delta\Delta ZPE/k_BT)]_{rem}$ = 0.442) for the MMI term of 2.45, and overcompensate when the EXC$_{rem}$ (0.760) is also considered. Nonetheless, it is informative to note that the main remnant contribution is a twisting mode at 597.3 (476.3) cm^{-1}, which represents a partial remnant of ethylene rotation about the carbon−carbon axis and produces a ZPE factor of 0.747 (Figure 7). In summary, if it can be assumed that the AMMI of Table 6 is applied to the EXP[$-(\Delta\Delta ZPE/k_BT)$]/EXP[$-(\Delta\Delta ZPE/k_BT)]_{rem}$ term (0.823 × 1.077 = 0.886), the standard interpretation of the inverse isotope effect on ethylene binding holds; the effect arises from increases in primarily out-of-plane bending vibrations on going from sp^2 to sp^3.

An important precedent for this ZPE analysis is found in Bender's investigation of the EIE for reversible binding of C_2H_4/C_2D_4 to $Os_2(CO)_8$, giving the diosmacyclobutane (μ-η^1,η^1-C_2H_4/C_2D_4)$Os_2(CO)_8$.[7] In this study, experimental vibrational frequencies for all isotopically sensitive normal modes were employed to compute individual EXC and ZPE contributions to the overall EIE. As in the EIE$_{calc}$ of **2′**-C_2H_4, the overall EXP[$-(\Delta\Delta ZPE/k_BT)$] term for this EIE is inverse (0.355), with the strongest contribution (0.525) arising from a twisting mode, with a frequency of 1012 (732) cm^{-1} corresponding to the remnant of ethylene rotation about the carbon−carbon axis. The second and third most significant ZPE contributors also parallel the **2′**-C_2H_4 case: an out-of-plane bending vibration (the b_{2g} combination in this instance) contributes a factor of 0.705, while the carbon−carbon stretch produces a contribution of 0.717.

Intramolecular EIEs. 1. MMI and Remnants. The MMI term for the intramolecular EIE cases is 1.00, because **1**-R and **1**-ND-R′ have the same mass and possess only minute differences in moments of inertia (note that the models **1′**-R etc. were not used in this context). As in the intermolecular cases, **1**-R and **1**-ND-R′ possess rotational and vibrational remnants that contribute significantly to the EXC and EXP[$-(\Delta\Delta ZPE/k_BT)$] terms, but in these intramolecular cases, the MMI counterpart is insignificant due to the absence of free hydrocarbon in the equilibrium.

2. EXC Term. The EXC contributions to the EIE$_{calc}$ fall in the relatively small range from 0.855 (**1′**-2,4,6-$C_6H_2D_3$) to 0.969 (**1′**-CH_2CD_3), and should be considered minor. The most important terms involve NH bending, where the in-plane modes contribute about 0.97 in both the inter- and intramolecular cases. Although the number of deuteriums is greater in each intermolecular case, the critical C−H/D bending vibrations of **1′**-R_H, **1′**-ND-R_D, R_HH, and R_DD are too high to be significant.

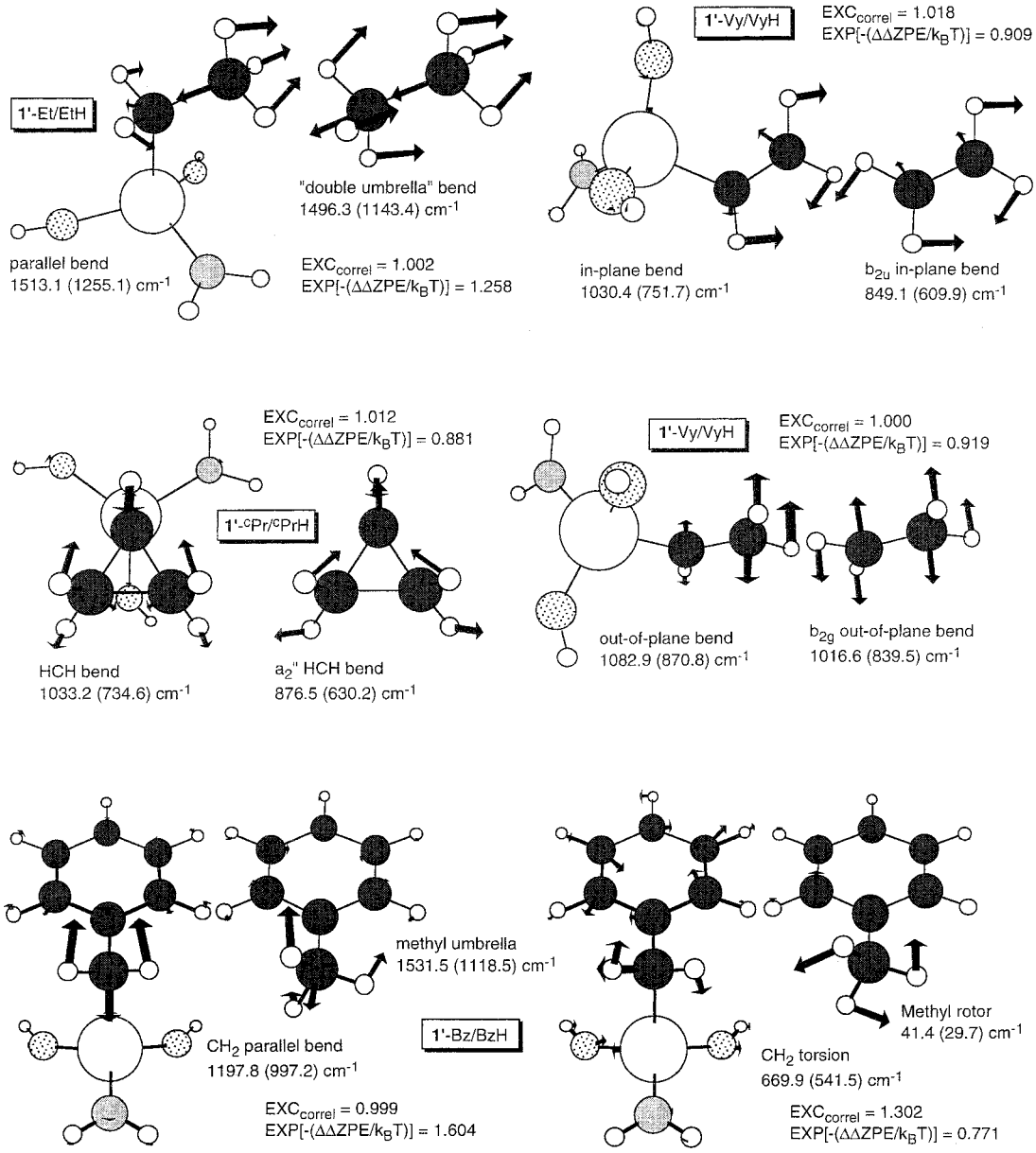

Figure 6. Some significant vibrations in **1′**-R_H (**1′**-ND-R_D) correlated with their R_HH (R_DD) counterparts.

The out-of-plane NH bending vibration is composed of lower energy vibrations (symmetric and antisymmetric, Figure 4) and contributes a greater inverse factor. There are subtle variations among R, and the intramolecular values (e.g., 0.865 (**1′**-CH_2-CD_3) to 0.941 (**1′**-2,2-$^cC_3H_3D_2$)) essentially track the intermolecular cases (e.g., 0.854 (**1′**-CH_2CD_3) to 0.943 (**1′**-2,4,6-$C_6H_2D_3$)), with the sp^2 R-groups having a slightly less inverse impact on EXC. Inspection of the vibrational frequencies reveals that the sp^3 substituents are generally higher than those of the sp^2 cases, but there is less mixing with lower frequency core vibrational modes in the sp^3 cases; hence their contribution to EXC is more substantial (i.e., $\Delta\nu$ is roughly greater for **1′**-R vs **1′**-ND-R′). In the case of **1′**-CH_2CD_3, this is offset by a 1.085 contribution from rotation about the C−C bond. As a corollary, the greater mixing between out-of-plane bends and core vibrations in the sp^2 cases is revealed by a more significantly inverse contribution among the core modes of **1′**-2,4,6-$C_6H_2D_3$ (0.921) and **1′**-2,2-$^cC_3H_3D_2$ (0.935) due to certain low-frequency modes. The benzyl case has a significantly inverse contribution (0.942) from core vibrations as well. The dominance of these factors is revealed in the EXC, where the latter three cases exhibit the most inverse of all the intramolecular examples (Table 4).

In summary, the EXC terms vary within ∼13% as a function of R and have only a minor impact on the intramolecular EIE_{calc} values. EXC is also not a significant factor in distinguishing inter- (as EXC/EXC_{rem}) and intramolecular examples, since their magnitudes are similar.

3. EXP[−(ΔΔZPE/k_BT)] Term. As in the intermolecular cases, factors of the EXP[−(ΔΔZPE/k_BT)] term are the most important contributors to EIE_{calc}. Certain types of vibrations are critical in determining the magnitude of EXP[−(ΔΔZPE/k_BT)], yet fail to distinguish between R; neither do these modes differentiate intra- from intermolecular factors. For example, the symmetric and antisymmetric $\exp(-h\nu^{1'-R}/2k_BT)$ $\exp(h\nu^{1'-(ND)-R'}/2k_BT)$ components pertaining to NH stretches afford a 0.0872(2) contribution to all intramolecular cases (one exception is **1′**-CHDPh, but the difference is due to $T = 50.0$ °C), and this factor is common to the intermolecular examples. Likewise, the in-plane NH bending contribution (symmetric and antisymmetric product) ranges from 0.5123 (**1′**-2,2-$^cC_3H_3D_2$) to

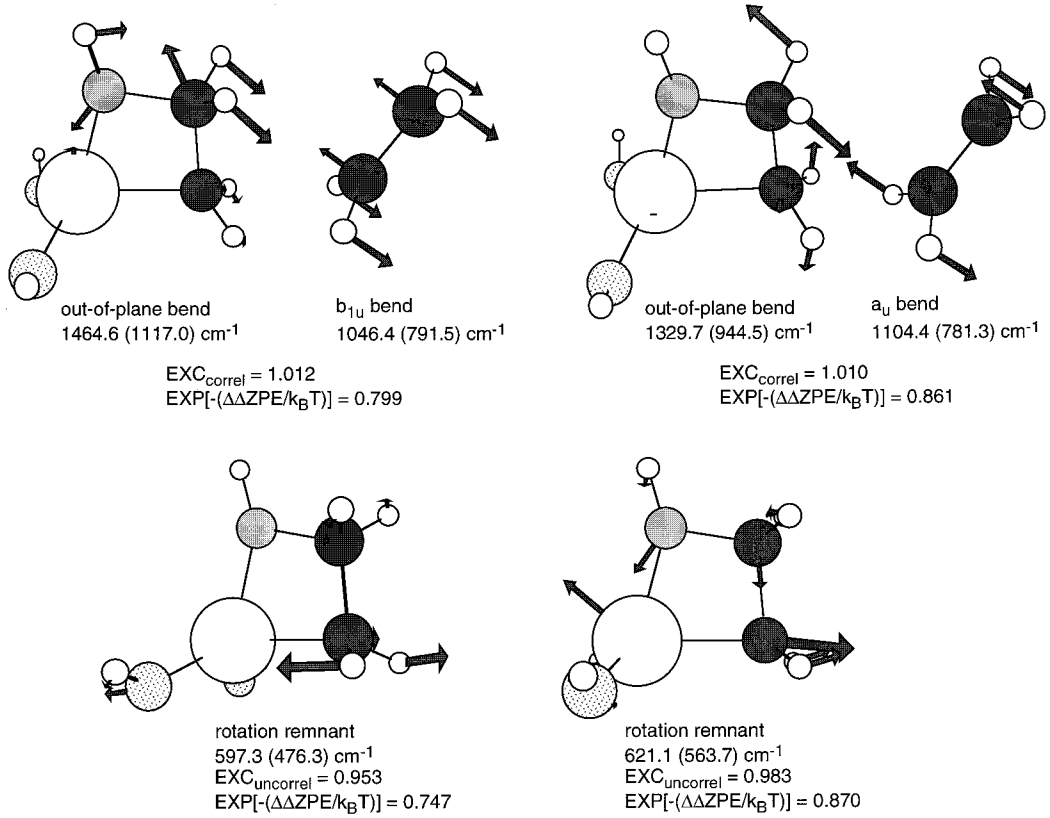

Figure 7. Some significant correlated and core vibrations of (silox)$_2$(^{t}Bu$_3$SiN)TiCH$_2$CH$_2$ (**2**-C$_2$H$_4$), modeled by (HO)$_2$(HN)TiCH$_2$CH$_2$ (**2′**-C$_2$H$_4$).

0.5238 (**1′**-DC=CDH) for the **1′**-R at 24.8 °C and tracks with the corresponding intermolecular cases (i.e., 0.5049, **1′**-^{c}C$_3$H$_5$; 0.5264, **1′**-HC=CH$_2$). Greater variation is observed in contributions from the out-of-plane NH bending vibrations, yet these factors are significantly less inverse, principally because the vibrations are of lower energy. These vary from 0.7865 for **1′**-CH$_2$CD$_3$ to 0.8815 for **1′**-2,2-^{c}C$_3$H$_3$D$_2$.

The products of the NH bending contributions are 0.407 (**1′**-CH$_2$CD$_3$), 0.431 (**1′**-CD=CHD), 0.434 (**1**-CD$_3$), 0.436 (**1′**-CH$_2$D), 0.438 (**1′**-CHD$_2$), 0.449 (**1′**-CHDPh), 0.452 (**1′**-2,2-^{c}C$_3$H$_3$D$_2$), and 0.454 (**1′**-2,4,6-C$_6$H$_2$D$_3$). They are within 10% and are each within their intermolecular counterparts by 5%. The remaining modes, predominantly CH bending, and to a lesser extent CH stretching and core vibrations, are the critical features to differentiating intramolecular EIEs on the basis of R. These factors, and the difference in the number of vibrations, provide the basis for distinguishing between intra- vs intermolecular cases.

4. Intramolecular Cases and Intermolecular Comparisons. The intramolecular cases feature an exchange of an −ND(−NH) bond for a −CH(−CD) bond within the same organometallic complex, whereas this exchange occurs with a substrate in the intermolecular examples. This difference has many ramifications, such as the contributions from CH stretching frequencies. Table 5 compiles various $\exp(-h\nu^{\mathbf{1}'-\mathrm{R}}/2k_BT)$ $\exp(h\nu^{\mathbf{1}'-(\mathrm{ND})-\mathrm{R}'}/2k_BT)$ product factors and enables a ready comparison with the intermolecular factors.

Less variation in EIE$_{calc}$ values is observed for the intramolecular cases, which range from 1.44 for **1′**-CH$_2$CD$_3$ to 0.867 for **1′**-CH$_2$D, but the interpretation essentially remains the same; differences are dominated by CH/D factors. Using the product of all CH and related factors (CH stretches, CH bends, internal rotations, and carbon-based vibrations), the following ranking of contributions to EXP[−(ΔΔZPE/k_BT)] can be made: **1′**-CH$_2$-CD$_3$ > **1′**-2,2-^{c}C$_3$H$_3$D$_2$ ~ **1′**-2,4,6-C$_6$H$_2$D$_3$ > **1′**-DC=CHD > **1′**-CHDPh > **1′**-CH$_n$D$_{3-n}$ (n = 0−2). The trend parallels the EIE$_{calc}$ values, thereby substantiating the importance of the CH factors to EXP[−(ΔΔZPE/k_BT)]. Critical contributions to each intramolecular EIE$_{calc}$ and a comparison to the corresponding intermolecular case are reviewed in turn.

a. 1-ND-CH$_x$D$_{3-x}$ ⇄ 1-CH$_{x-1}$D$_{4-x}$ (x = 1−3). The EIE$_{calc}$/SYM values corresponding to the three isotopologues of methane are essentially the same (0.90(3)) and are approximately half that of the intermolecular EIE$_{calc}$ = 1.88. Because of the necessity of correlating CH$_4$, **1′**-CH$_3$, CD$_4$, and **1′**-ND-CD$_3$ in the intermolecular cases, there is not a simple one-to-one correspondence between these CH contributions and the intramolecular analogues. For example, in the CH$_2$D$_2$ intramolecular case, two stretches provide mildly normal contributions; one that is effectively a CD mode in both product **1′**-ND-CH$_2$D and reactant **1′**-CHD$_2$, and another that is essentially a CH mode. Combined with the CD (product) for CH (reactant) exchange that provides a 6.531 normal contribution, the CH contributions give a factor of 7.992. In the intermolecular example, three CH stretches of reactant CH$_4$ correlate with product **1′**-CH$_3$, and three CD stretches of reactant **1′**-ND-CD$_3$ correlate with product CD$_4$ to afford a 1.163 normal factor. The remaining CD/H stretch correlates with the NH/D stretch; hence it is the pure contribution from product CD$_4$ vs reactant CH$_4$ that affords 7.809 toward the EXP[−(ΔΔZPE/k_BT)] contribution. Overall, the stretches generate a greater normal contribution of 9.082 for the intermolecular case in contrast to the 7.992 of the intramolecular example, predominantly because the free hydrocarbon contributions are normal and CD$_4$ is a product. The remaining isotopologues can be similarly compared.

In the case of the bending vibrations, the CD$_4$ product is even more consequential in the intermolecular case. This intermolecular uncorrelated CH contribution (a single bending vibration) of 2.345 (CD$_4$ vs CH$_4$, Figure 5) is augmented by correlated contributions (CH$_4$ vs **1′**-CH$_3$ and CD$_4$ vs **1′**-CD$_3$) whose product

is 1.596. Factors of 2.263, 2.475, and 2.730 stem from the **1′**-CH_2D (vs **1′**-ND-CH_3, etc.), **1′**-CHD_2, and **1′**-CD_3, intramolecular cases, and mode mixing ensures that each of the three bends provides a normal contribution in all cases. At this point, the EIE values of the intra- and intermolecular cases are not too far apart, *but another CH bending vibration remains to be counted in the intermolecular example.* The CD_4 vs CH_4 bending contribution that correlates with the NH out-of-plane bends provides another factor of 2.345, thereby revealing the origin of the substantial difference in intramolecular and intermolecular EIE_{calc} values. Core vibrations, some of which correspond to rotational and translational remnants, provide a normal contribution of 1.288 for the intramolecular CH_2D_2 case, but the most important distinguishing vibrations are clearly the CH bends.

b. 1-ND-CD_2CH_3 ⇄ 1-CH_2CD_3. A single isotopologue, H_3CCD_3, was used to investigate the intramolecular isotope effect accorded ethane. Differences between inter- and intramolecular EIEs are at a maximum in the methane case, but are still significant in most of the remaining instances. In ethane, the intermolecular EIE_{calc} of 1.93 is greater than the 1.44 calculated for substrate CH_3CD_3.

A large normal contribution of 8.393 is provided by CH(D) stretches, since there are three CD bonds in the product and only two in the reactant. This contribution contains an additional small normal factor that reflects the more strongly bound CH(D) bonds of the β-position relative to α-positions. In the intermolecular case, correlated CH(D) stretches afford a normal 1.163 contribution, while the uncorrelated CH(D) factor (eq 26) derived solely from a single stretch of the hydrocarbon is 7.714. As a consequence of CH stretches, the intermolecular EIE_{calc} is greater than the intramolecular one by 8.802 vs 8.393.

Bending vibrations perpendicular to the C−C axis account for a 3.417 factor toward $EXP[-(\Delta\Delta ZPE/k_BT)]$ in the intramolecular case, principally because two of the three are significantly isotope dependent and favor deuterium in the β-position, while the remaining mode is opposite in character and inverse. The related intermolecular in-plane bends contribute somewhat less. Due to the C_2D_6 product and its generally higher frequency vibrations, the correlated CH(D) bends (eq 24) generate a normal contribution of 1.097. The single CH(D) bend of C_2H_6(C_2D_6) contributes 2.910 (Figure 5) for a product of 3.192.

Bending vibrations parallel to the C−C axis are a key feature in differentiating inter- from intramolecular ethane EIEs. In the intramolecular case, a single parallel bend that favors deuterium in the β-position (2.122) is offset by several moderately inverse contributions, leading to a product of 1.512. The intermolecular case is again distinguished by a substrate bend correlating with the out-of-plane NH bend. It contributes 1.871, and is augmented by correlated factors whose product is 1.094.

Internal rotation about the C−C bond provides essentially the same factor in both cases, but contributions from the slightly isotopically sensitive C−C stretch are slightly greater for the intramolecular case (1.173 vs 1.045). Core vibrations are substantively inverse (0.759) for the intramolecular case, since the isotopic sensitivity derives from deuteriums in α-positions. In summary, the intermolecular EIE_{calc} is greater than its intramolecular relative primarily due to C_2D_6 vs C_2H_6 parallel bends, intermolecular CH stretching contributions, and core vibrations that favor the reactant **1′**-ND-CD_2CH_3 vs product **1′**-CH_2CD_3 in the intramolecular case.

c. 1-ND-$^cC_3H_4D$ ⇄ 1-$^cC_3H_3D_2$. Use of 1,1-$^cC_3H_4D_2$ afforded a EIE_{calc}/SYM of 1.27 for the intramolecular case in comparison to the intermolecular value of 1.48. The distinction between the two is subtle, and the aforementioned comparisons that were used in the cases above are all relevant. CH(D) stretching vibration contributions are 8.828 (1.139 from correlated, i.e., eq 24; 7.751 from the uncorrelated substrate component, eq 26) in the intermolecular case, while the intramolecular stretching contributions are 8.546. In the intermolecular example, correlated bending vibrations perpendicular to the C_3 plane contribute less (0.929) than those in the intramolecular case (0.990), principally because an a_2'' substrate bend exists at somewhat higher energy in the bound form. A major contribution (2.601, Figure 5) stems from the uncorrelated substrate component in the intermolecular case. Bending contributions from vibrations parallel to the C_3 plane have a notedly different effect on the intra- and intermolecular EIE_{calc} values. Correlated CH components of the intermolecular example effectively cancel (1.0118), while the uncorrelated factor of eq 26 contributes 1.466, again due solely to the differences in product $^cC_3D_6$ vs reactant $^cC_3H_6$ (Figure 5). Contributions from this bend in intramolecular product **1′**-2,2-$^cC_3H_3D_2$ vs reactant **1′**-ND-1-$^cC_3H_4D$ are augmented by higher frequency bends that involve β-deuteriums, leading to a 1.980 normal contribution. The $EXP[-(\Delta\Delta ZPE/k_BT)]$ term is further increased by a large 2.401 contribution from ring breathing and distortion modes. These are moderately isotopically sensitive (1.332) in the correlated intermolecular case, but are highly sensitive in the uncorrelated intramolecular case due to the asymmetry of isotopic substitution and correspondingly greater degree of mixing with CH bending modes. Core vibrational contributions attentuate the $EXP[-(\Delta\Delta ZPE/k_BT)]$ term by 0.918 in the intramolecular case. Clearly, it would have been difficult to predict the origins of the differences between the inter- and intramolecular EIEs without the aid of calculations.

d. 1-ND-*trans*-CH═CHD ⇄ 1-*trans*-CD═CHD. The intramolecular EIE_{calc} of 1.00 is moderately less than the 1.34 calculated for the intermolecular case. The CH stretching components behave much as in the previous cases, and the product of correlated and uncorrelated terms in the intermolecular case is 8.980—greater than the 8.023 of the intramolecular example. The product (2.300) of contributions from correlated (0.882) and uncorrelated (2.607, Figure 5) out-of-plane bending vibrations in the intermolecular case is slightly greater than that in the intramolecular example (2.195). Similarly, correlated (0.974) and uncorrelated (1.851, Figure 5) contributions from in-plane bends in the intermolecular case are also slightly larger than the corresponding intramolecular contribution (1.697). The C═C stretch provides a normal contribution in both the intermolecular (correlated, 1.133) and intramolecular (1.034) cases, while core vibrations attenuate the intramolecular $EXP[-(\Delta\Delta ZPE/k_BT)]$ term by 0.925. In virtually all categories, each type of vibration is slightly greater for the intermolecular example; hence no mode stands out as the dominant contributor to the difference in inter- vs intramolecular EIEs.

e. 1-ND-3,5-$C_6H_3D_2$ ⇄ 1-2,4,6-$C_6H_2D_3$. The EIE_{calc} values for the intramolecular (1.25) and intermolecular (1.26) cases involving benzene are virtually identical due to an interesting cancelation of certain contributions. The CH stretching components are very similar in the two examples; the product of correlated and uncorrelated terms in the intermolecular case is 8.360, only slightly greater than the 8.208 of the intramolecular example. However, the product of the out-of-plane correlated (1.013) and in-plane uncorrelated (2.265, Figure 5) bends in the intermolecular case is significantly greater than the 1.292 accorded the intramolecular example, whose magnitude is derived primarily from a single "a_{2g}"-type vibration that

Table 7. Experimentally Inferred Intermolecular (R_HH vs R_DD) and Intramolecular (RH vs R′D, RH = R′D) Kinetic Isotope Effects (KIE_{addn}) for 1,2-Hydrocarbon-Addition to (silox)$_2$Ti=NSi^{t}Bu$_3$ (**2**)[a,b]

intermol. R_HH/R_DD	intramol. RH/R′D	EIE_{obs}/SYM	EIE_{calc}/SYM	KIE_{elim}	KIE_{addn}(exptl)[c]	KIE_{addn}(calcd)[c]
CH_4/CD_4		2.00(6)	1.88	14.7(17)[d]	29.4(35)[d]	27.6[d]
	CDH_3	1.05(8)	0.87	13.4(10)[e]	14.1(15)[e]	11.7[e]
	CD_2H_2	1.13(8)	0.91		15.1(16)[e]	12.2[e]
	CD_3H	1.17(7)	0.91		15.7(15)[e]	12.2[e]
C_2H_6/C_2D_6		2.22(8)	1.93	14.3(7)	31.7(19)	27.6
	CD_3CH_3	1.53(3)	1.44		21.9(12)	20.6
$^cC_3H_6/^cC_3D_6$		1.71(4)	1.48	9.0(5)	15.4(9)	13.3
	1,1-$^cC_3H_4D_2$	1.29(3)	1.27		11.6(7)	11.4
$H_2C=CH_2/D_2C=CD_2$		1.41(11)	1.34	7.8(4)	11.0(10)	10.5
	trans-HDC=CHD	1.00(2)	1.00		7.8(4)	7.8
C_6H_6/C_6D_6		1.22(7)	1.26	7.4(3)	9.0(6)	9.3
	1,3,5-$C_6H_3D_3$	1.273(4)	1.25		9.4(4)	9.3
C_7H_8/C_7D_8[f]		1.59(6)	1.55	10.5(7)[f]	16.7(13)	16.3
	$PhCH_2D$	1.03(1)	0.99		10.8(7)	10.4

[a] All KIE_{elim} values refer to k_H/k_D, where k_H refers to the 1,2-R_HH-elimination from (silox)$_2$(^{t}Bu$_3$SiNH)TiR_H (**1**−R_H) and k_D refers to 1,2-R_HD-elimination from (silox)$_2$(^{t}Bu$_3$SiND)TiR_H (**1**−ND-R_H). This assumes secondary effects on the elimination reaction are not substantial (see text). [b] EIE_{obs} at 26.5(3), EIE_{calc} at 24.8 °C; KIE_{elim} at 24.8(3)°C for **1**−R vs **1**−ND-R′, R = Me, Ph, CH_2Ph; KIE_{elim} at 26.5 °C for R = Et, CH=CH_2 and ^{c}Pr. [c] All inferred KIE_{addn}(exptl) values calculated according to eq 8 using the EIE_{obs}/SYM and the experimental KIE_{elim}; all KIE_{addn}(calcd) values calculated using EIE_{calc}/SYM and the experimental KIE_{elim}. [d] Obtained by multiplying the KIE for **1**-CH_3 vs **1**−ND-CH_3 elimination (13.7(9)) by the KIE for **1**-CH_3 vs **1**-CD_3 elimination (1.07(10)); for comparison to the other **1**-R, exclusion of the secondary KIE yields KIE_{addn}(exptl) = 27.4(20) and KIE_{addn}(calcd) = 25.8. [e] Obtained by dividing the KIE for **1**-CH_3 vs **1**-ND-CH_3 elimination (13.7(9)) by the KIE for **1**-$CH_{3-x}D_x$ (x = 0−2) vs **1**-$CH_{2-x}D_{x+1}$ elimination (1.02(3)); for comparison to the other **1**-R, exclusion of the secondary KIE yields KIE_{addn}(exptl/calcd) = 14.4(14)/11.9 for x = 0, 15.5(15)/12.5 for x = 1, and 16.0(14)/12.5 for x = 2. [f] EIE_{obs} at 50.0 (3)°C; KIE_{elim} at 52.4 (3)°C.

contributes 1.405. As in the previous cases, the intermolecular uncorrelated 2.265 component derives solely from an e_{2g} bend in product C_6D_6 vs reactant C_6H_6. Out-of-plane bends are not very different in the two cases. Intermolecular correlated contributions are slightly inverse (0.983), and the uncorrelated substrate component is 1.669 (Figure 5). The product of the intramolecular out-of-plane bends is 1.885, with a single "e_{2u}"-type mode responsible for a 1.607 factor.

The greater normal product accumulated thus far in the intermolecular case is counteracted by a single in-plane ring distortion of an "e_{1u}" type that contributes 1.920 to an overall product of 2.013 from all ring vibrations in the intramolecular example. The intermolecular contribution from ring modes is also normal, but with only a 1.215 product. The intramolecular EXP[−($\Delta\Delta$ZPE/k_BT)] term is again attenuated (0.918) by core vibrations, but the counteraction of the perpendicular CH bends and the ring vibrations leads to nearly equal zero-point contributions in the inter- and intramolecular cases.

f. 1-ND-CH_2Ph ⇄ 1-CHDPh; 50.0 °C. In the final example, the intermolecular EIE_{calc} of 1.55 is substantially greater than the intramolecular EIE_{calc}/SYM of 0.99 for the substrate toluene. The CH stretching vibrations do not play a dramatic role in differentiating the inter- and intramolecular cases. The product of correlated and uncorrelated intermolecular contributions (7.074) is slightly greater than the intramolecular product of 6.616. The uncorrelated perpendicular bend (the factor in eq 27) in the intermolecular case contributes 2.765 due to the $-CD_2-$ vs $-CH_2-$ bends of C_7D_8 vs C_7H_8 (Figure 5), and while this is slightly attentuated by factors (0.966) from correlated bends, it is substantially greater than the normal contribution (1.425) in the intramolecular case. The latter arises almost solely from the product $-CD_2-$ vs the reactant CHD perpendicular bending contribution of 1.400. The uncorrelated parallel bend derived from CD_2/CH_2 as above contributes 1.497, and the correlated contributions are also significantly normal, providing an additional factor of 1.576. In combination, they are significantly greater than the intramolecular parallel bend factor of 1.627. The difference in the correlated perpendicular vs correlated parallel contributions in the intermolecular case is symmetry related. For the perpendicular bends, a difference in symmetry between the correlated and uncorrelated contributions minimizes any mixing, but in the parallel bends this problem is absent, and significant mixing ensues.

The Me-Ph rotation is the origin of a very large difference in EXP[−($\Delta\Delta$ZPE/k_BT)] factors. In the intermolecular case, this correlated term is dominated by **1′**-$CD_2C_6D_5$, whose substantially higher frequency vs that of toluene-d_8 generates an inverse correlated factor of 0.771 (Figure 6). The same rotor is responsible for a 1.300 normal contribution in the intramolecular case due to the presence of deuterium on the methylene group of **1′**-CHDPh. Due to some mixing of ring vibrations with the methylene group, ring breathing and deformation vibrations yield normal factors toward the inter- and intramolecular EXP[−($\Delta\Delta$ZPE/k_BT)], but the intramolecular contribution of 1.271 is substantially greater than the intermolecular one of 1.040. Core vibrations provide an additional factor of 0.942 to the intramolecular case. In summary, the internal rotor and various carbon-based vibrations generate greater factors in the intramolecular case, but CH stretches and bends provide greater contributions in the intermolecular example, leading to its greater EXP[−($\Delta\Delta$ZPE/k_BT)]/EXP[−($\Delta\Delta$ZPE/k_BT)]$_{rem}$ term and a greater EIE_{calc}.

Kinetic Isotope Effects for 1,2-Hydrocarbon-Addition to (silox)$_2$Ti=NSi^{t}Bu$_3$ (2). 1. Background. From Scheme 1 and eq 8, it can be seen that k_H/k_D for the 1,2-R_HH-addition vs 1,2-R_DD-addition to (silox)$_2$Ti=NSi^{t}Bu$_3$ (**2**) can be inferred as EIE × KIE_{elim}. Likewise, the intramolecular equivalent, KIE_{addn} = k_H/k_D for 1,2-($C_zH_{x-1}D_y$)H-addition vs 1,2-($C_zH_xD_{y-1}$)D-addition, can also be determined via EIE × KIE_{elim}. In practice, the ratios of elimination rates from various **1**-R and **1**-ND-R were measured, and secondary effects were assumed to be minimal in the addition step, as was determined from the aforementioned experiments involving **1**-CH_3 vs **1**-CD_3. As a consequence, for each hydrocarbyl species the same KIE_{elim} was applied to most of the inter- and intramolecular EIEs to obtain the 1,2-addition KIEs.

Table 7 provides the experimentally inferred inter- and intramolecular KIE_{addn} values, and their "calculated" counterparts, where EIE_{calc} is used in eq 8 rather than the experimental EIEs. Given the assumption regarding secondary effects above, the difference in inter- and intramolecular KIE_{addn} values is the factor provided by EIE_{obs} or EIE_{calc} for the respective cases. It

would also seem likely that similar factors, i.e., predominantly $EXP[-(\Delta\Delta ZPE/k_BT)]$ terms, especially bending modes, distinguish KIE_{addn}(inter) from KIE_{addn}(intra). To discuss the KIE_{addn} values, eq 28 will be examined as representing the intermolecular k_H(addn)/k_D(addn), with $Q(R_HH) = Q_{rot}(R_HH)Q_{tr}(R_HH)Q_{vib}(R_HH)$, $Q(L_nM(R_HH)^{\ddagger}) = Q_{rot}(L_nM(R_HH)^{\ddagger})Q_{tr}(L_nM(R_HH)^{\ddagger})Q_{vib}(L_nM(R_HH)^{\ddagger})$, and $\Delta\Delta ZPE = (ZPE(L_nM(R_HH)^{\ddagger}) - ZPE(L_nM(R_DD)^{\ddagger}) + (ZPE(R_DD) - ZPE(R_HH))$. The expression

$$\frac{k_H(addn)}{k_D(addn)} = \frac{\kappa_H Q(R_DD)Q(L_nM(R_HH)^{\ddagger})}{\kappa_D Q(R_HH)Q(L_nM(R_DD)^{\ddagger})} \times EXP[-(\Delta\Delta ZPE/k_BT)] \quad (28)$$

and definitions (κ_H and κ_D are transmission coefficients assumed to be the same) are the same as those presented in eqs 4−7, except that a single vibration has become the reaction coordinate such that $ZPE(L_nM(R_HH)^{\ddagger}) = \Sigma_i^{3n-7}(h\nu_i/2)$.[1−4,33] From the formalism, the same MMI term is operational in the intermolecular EIE and the KIE_{addn}, and it is likely that it will be counteracted by the same compensating factors, the EXC_{rem} and $EXP[-(\Delta\Delta ZPE/k_BT)]_{rem}$ terms.

Bender looked at the EIE for methane binding (CH_4 vs CD_4) to an $OsCl_2(PH_3)_2$ fragment, using calculations by Avdeev and Zhidomirov in the process.[31] He found that the product of EXC_{rem} and $EXP[-(\Delta\Delta ZPE/k_BT)]_{rem}$ terms (0.185) again more than compensates for the 3.95 MMI term. Assuming that this weak complex can be considered a transition state model for methane binding, at least from the standpoint of energetics, the data substantiate the claim that compensation by EXC_{rem} and $EXP[-(\Delta\Delta ZPE/k_BT)]_{rem}$ terms is general to EIE and KIE cases.

For the intramolecular cases, eq 29 (RH = R′D) reveals no consequential MMI term, since the substrate is common to both CH- and CD-activation transition states, and the comparison between KIE_{addn}(intra) and KIE_{addn}(inter) parallels the EIE discussion. Now $\Delta\Delta ZPE = (ZPE(L_nM(RH)^{\ddagger}) - ZPE(L_nM(R'D)^{\ddagger})$; hence the zero-point energy term depends only on vibrational frequencies of the two transition states.

$$\frac{k_H(addn)}{k_D(addn)} = \frac{\kappa_H Q(L_nM(RH)^{\ddagger})}{\kappa_D Q(L_nM(R'D)^{\ddagger})} \times EXP[-(\Delta\Delta ZPE/k_BT)] \quad (29)$$

2. 1,2-Hydrocarbon-Elimination KIE_{elim} Values. The values determined for **1**-CH_2CH_3 vs **1**-ND-CH_2CH_3, **1**-^{c}Pr vs **1**-ND-^{c}Pr, and **1**-CH=CH_2 vs **1**-ND-CH=CH_2 supplement the trend observed previously for the remaining cases. Transition states that occur earlier along the 1,2-RH-elimination reaction coordinate, which are typified by sp^3 substrates, manifest greater KIE_{elim} values than those occurring later. Two factors are responsible for **1**-R (R = sp^2-hybridized) having substantially later transition states: ground states of the sp^2-hybridized alkyls are lower in energy than their sp^3 congeners, and the 1,2-elimination reaction coordinate is compressed for sp^2- relative to sp^3-hybridized substituents.[17]

3. Inter- and Intramolecular KIE_{addn} Values. As a corollary to the previous 1,2-RH-elimination arguments, KIE_{addn} values that correspond to transition states that are earlier in the 1,2-RH-addition reaction coordinate will be less symmetric than those occurring later and will be smaller in magnitude. This follows naturally from the exoergocity of the 1,2-addition event.[17] The intermolecular KIE_{addn} values scale accordingly: ethane > methane > toluene (benzyl) > cyclopropane > ethylene > benzene. While there is some variation within the intramolecular complements, in part due to their lesser magnitudes, the trend is still the expected sp^3 (RH) > sp^2.

The magnitudes of KIE_{addn}(exptl) values are substantial, with intermolecular ethane and methane values of 31.7(19) and 29.4(35), respectively. Even when the lesser and perhaps more accurate EIE_{calc} values are used to calculate the intermolecular values, KIE_{addn}(calcd) for the sp^3 substrates is still 27.6, a number that exceeds typical predictions based on prototypical models of organic transformations.[1−4] Even the lowest of the intermolecular KIE_{addn} values, the 9.0(6) accorded activation of C_6H_6 vs C_6D_6, would normally be considered a large primary effect, and the "intermediate" values of 16.7(13), 15.4(9), and 11.0(10) assigned to the toluene, cyclopropane, and ethylene cases would be considered extraordinary. Furthermore, since the EIEs essentially matched the EIE_{calc} values, and the KIE_{elim} values fall within a standard—albeit high—range, it is not necessary to invoke additional mechanisms such as hydrogen atom tunneling to explain the KIE_{addn} values. Clearly, the higher and more limited range of vibrational frequencies encountered in a typical organic reaction constrains primary isotope effects to a moderate scope, whereas transition metal systems, which contain a host of oscillators coupled to the metal to varying degrees, can exhibit greater variation and substantially greater magnitudes. For instance, the F_3CO_2H/F_3CO_2D-catalyzed isomerization of {η^4-(1,5-diphenyl,1-*trans*,3-*cis*-pentadiene)}$Fe(CO)_3$ to {η^4-(1,5-diphenyl,1-*trans*,3-*trans*-pentadiene)}$Fe(CO)_3$ occurs with a KIE of 27(1).[34] Consequences of the change in vibrational frequencies associated with the proton transfer between oxygen and metal in this intermolecular KIE may parallel those discussed herein.

Without calculation of the various transition states for 1,2-RH-addition,[35] it is difficult to detail the critical features of the C−H bond activation events, and therefore the KIE_{addn} values. Nonetheless, similar features that differentiate inter- from intramolecular EIEs must also be operational in the kinetic isotope effects. As eqs 28 and 29 indicate, disparities between inter- and intramolecular KIE_{addn} values are probably due to the differing degrees of counterbalancing that occur when $EXP[-(\Delta\Delta ZPE/k_BT)]$ contributions from correlated transition-state vibrations are opposed by substrate factors (intermolecular) versus cases when transition-state vibrations involving different amounts of deuterium motion oppose one another (intramolecular). Given the importance of the correlated NH bending modes in the EIEs, which are matched by corresponding substrate CH vibrations in the inter- but not the intramolecular cases, bending vibrations in 1,2-RH-addition transition states involving NH motion will be critical. All of these factors fall under the aegis of "primary" effects; hence vibrations that constitute the "secondary" effects are expected to have minimal impact.

In the cases herein, the unpredictability of inter- vs intramolecular KIE_{addn} values can be readily observed. For methane, the intramolecular CDH_3 (14.1(15)), CD_2H_2 (15.1(16)), and CD_3H (15.7(15)) cases are about half their intermolecular complement, while the 9.4(4) observed for CH- vs CD-addition of 1,3,5-$C_6H_3D_3$ is within error of the intermolecular value. For the remaining cases, the intramolecular value is ~70% of the intermolecular KIE_{addn}(exptl).

4. Relevance to Other Transition Metal Systems. The most relevant case of addition KIEs concerns the activation of methane by transient $(^tBu_3SiNH)_2Zr$=NSi^tBu_3. Direct measure-

(33) Bigeleisen, J. *J. Chem. Phys.* **1949**, *17*, 675−678.

(34) Whitesides, T. H.; Neilan, J. P. *J. Am. Chem. Soc.* **1975**, *97*, 907−908.

(35) Klinckman, T. R.; Cundari, T. R., work in progress.

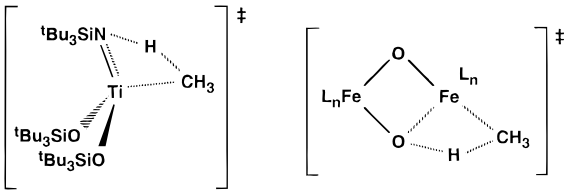

Figure 8. Sketch of the four-center MMO methane activation transition state as proposed by Yoshizawa, and the related transition state for CH-bond activation by transient (silox)$_2$Ti=NSi^{t}Bu$_3$ (**2**).

ment of the KIE$_{addn}$ values in this system shows a strong parallel with the titanium methane case presented here. The intermolecular KIE$_{addn}$ was 11.2(17) at 95.0 °C, a value roughly double that of its intramolecular counterparts: CDH_3, 6.1(3); CD_2H_2, 5.1(6); CD_3H, 3.7(7).[13] The magnitudes in the zirconium system are lower, but the transition states in these CH/D activation events are predicted to be somewhat less symmetric than in the titanium cases,[20] and the effects are diminished by the higher temperature. Given the calculated intermolecular EIE for this system (EIE$_{calc}$(Zr inter) = 1.7), the implied KIE for 1,2-CH_4/CD_4-elimination of 11.2/1.7 = 6.6 (17) is within reason of the measured KIE for elimination of 8.3(6).

Kinetic isotope effects on methane and related hydrocarbon activations by metalloenzymes have played a provocative role in mechanistic interpretations. In particular, methane activation by soluble methane monoxygenases (sMMO's), which apparently contain an Fe−O−Fe active functionality,[36] is characterized by extraordinarily large KIEs. Nesheim and Lipscomb

$$CH_4 + O_2 + NADH + H^+ \xrightarrow{sMMO} CH_3OH + H_2O + NAD^+ \quad (30)$$

reported a KIE of ∼50−100 for the hydroxylation of CH_4 vs CD_4 by sMMO isolated from *Methylosinus trichosporium* OB3b,[37] while Lippard et al. found a similarly large KIE of ∼28 for the same reaction in sMMO from *Methylococcus capsulatus* (Bath).[38] Since these KIEs are greater than those expected on the basis of typical physical organic interpretations,[1−4] a hydrogen tunneling[39] mechanism has been given credence.

In the system presented herein, a similarly high KIE$_{addn}$(exp/calc) = 29.4/27.6 for CH_4 vs CD_4 activation was observed and interpreted using a conventional approach. In view of this system, it is plausible that conventional arguments (eq 28) can be used to explain a significant fraction, or perhaps all of the magnitude of the KIEs pertaining to activations by sMMO. According to Yoshizawa et al., the titanium imide activations may be related to those of sMMO.[40] Density functional theory calculations on sMMO model complexes suggest that methane oxidation occurs via complexation followed by a four-center transition state that transfers a methyl group to Fe and a H to the μ-oxo ligand. As Figure 8 illustrates, the activation event bears some similarity to the purported transition state for 1,2-RH-addition to (silox)$_2$Ti=NSi^{t}Bu$_3$ (**2**).

Soybean lipoxygenase (SLO) is another metalloenzyme highlighted by large isotope effects on the oxidation of 9,12-(*Z*,*Z*)-octadecadienoic acid (linoleic acid = LA) to 13-hydroperoxy-9,11-(*Z*,*E*)-octadecadienoic acid. Values of 27.4(38)[41] and 28(2) (25(1) °C, pH = 9)[42] have been independently obtained, and additional experiments suggest that a range of KIEs from 20 to 80 may characterize the oxidation under [LA]-dependent conditions, and that the KIEs increase when the temperature is raised.[41] Related experiments involving HPLC detection of LA oxidation by human 15-lipoxygenase (15-HLO) reveal a KIE of 47(7) at 38 °C, which is comparable to the 48(5) measured for SLO.[43] Tunneling contributions have been invoked as a possible explanation for the large effects in these systems,[39] but given the complexity of events in lipoxygenase oxidation, and the likelihood that KIEs of 20−30 can be conventionally explained, it is plausible that a combination of mechanistic factors and normal vibrational interpretations may be enough to rationalize their magnitudes.

Conversely, and with respect to advocates of tunneling for describing situations of extraordinarily high KIEs, it is conceivable that such a factor is operational in this system. However, examination of mechanistically similar KIE$_{elim}$ values obtained for **1**-NH/D-CH_3 (13.7(9), 24.8 °C),[17] (^{t}Bu$_3$SiNH/D)$_3$ZrCH_3 (6.27(8), 96.7 °C),[12] (^{t}Bu$_3$SiNH/D)$_2$(^{t}Bu$_3$SiN=)TaCH_3 (>3.4(8), 182.8 °C)[15] reveals a temperature dependence—albeit among different systems—consistent with classical behavior. While tunneling processes may also exhibit similar temperature dependencies,[44] it is important to note that a conventional assessment is applicable.

Furthermore, in viewing the KIE$_{elim}$ values, the complete loss of an NH stretch to the reaction coordinate (eq 28) would provide a factor of ∼11 (298 K), and various factors from bending and lesser vibrations could attenuate or multiply this value to obtain the range of elimination KIEs measured. How can the conventional explanation rationalize KIE$_{addn}$ values approaching 30? A perusal of eq 28 indicates that the free hydrocarbons play a similar role as in eq 4, as they must since EIE = (KIE$_{addn}$)/(KIE$_{elim}$) (eq 8). Recall that section 4 revealed that the disparities in inter- and intramolecular EIE are dominated by a substrate bending vibration. *This same substrate vibration is at the origin of the differences in inter- vs intramolecular KIE$_{addn}$ values*. As a consequence, the intermolecular KIE$_{addn}$ contains a factor of ∼7.5 for the asymmetric CH/D stretch lost to the reaction coordinate that is augmented by (1) factors due to bending and lesser vibrations and (2) the critical substrate vibration. For example, in the CH_4/CD_4 case the EIE = {(7.5)(bend/other contrib.)(2.345)}/{(∼11)(bend/other contrib.)} ≈ 1.6, which approaches the EIE$_{calc}$ of 1.88. It is reasonable to conclude that the net contributions from bending and other vibrations will be normal—assuming a rather loose transition state—in both the forward (addn) and reverse (elim) reactions, thereby providing the necessary magnitudes of KIE$_{addn}$ and KIE$_{elim}$ without the need to invoke tunneling.

The EXP[−(ΔΔZPE/k_BT)] analysis for the EIEs herein revealed that exchange of a substrate CH bond for an amide NH bond results in NH bending vibrations that are lower in frequency than the "lost" substrate CH bending vibrations. The normal EXP[−(ΔΔZPE/k_BT)] contributions thus produced more

(36) (a) Que, L., Jr.; Dong, Y. *Acc. Chem. Res.* **1996**, *29*, 190−196. (b) Zheng, H.; Zang, Y.; Dong, Y.; Young, V. G., Jr.; Que, L., Jr. *J. Am. Chem. Soc.* **1999**, *121*, 2226−2235. (c) Hsu, H.-F.; Dong, Y.; Shu, L.; Young, V. G., Jr.; Que, L., Jr. *J. Am. Chem. Soc.* **1999**, *121*, 5230−5237.

(37) Nesheim, J. C.; Lipscomb, J. D. *Biochemistry* **1996**, *35*, 10240−10247.

(38) Valentine, A. M.; Stahl, S. S.; Lippard, S. J. *J. Am. Chem. Soc.* **1999**, *121*, 3876−3887.

(39) Bell, R. P. *The Tunnel Effect in Chemistry*; Chapman and Hall: New York, 1980.

(40) Yoshizawa, K.; Ohta, T.; Yamabe, T. *Bull. Chem. Soc. Jpn.* **1998**, *71*, 1899−1909.

(41) (a) Glickman, M. H.; Wiseman, J. S.; Klinman, J. P. *J. Am. Chem. Soc.* **1994**, *116*, 793−794. (b) Glickman, M. H.; Klinman, J. P. *Biochemistry* **1995**, *34*, 14077−14092.

(42) Hwang, C.-C.; Grissom, C. B. *J. Am. Chem. Soc.* **1994**, *116*, 795−796.

(43) Lewis, E. R.; Johansen, E.; Holman, T. R. *J. Am. Chem. Soc.* **1999**, *121*, 1395−1396.

(44) Borgis, D.; Hynes, J. T. *J. Phys. Chem.* **1996**, *100*, 1118−1128.

than compensate for inverse factors arising from replacement of one substrate CH stretch with a higher frequency NH stretch. Similarly, in the CH activation event, transition-state bending modes involving the transferred hydrogen acquire some heteroatom character, and would be expected to have lower frequencies than the free substrate bending modes with which they correlate. If these bending frequencies drop substantially in the transition state, they can provide the necessary augmentation to afford KIE_{addn} and KIE_{elim} values beyond the organic semiclassical limit. In summary, activation of CH bonds by heteroatom-containing functionalities, especially those whose transition states are symmetric—not particularly "early" or "late"—are attractive candidates for the observation of extraordinarily large KIEs.

Conclusions

On the basis of this combined experimental and computational assessment of equilibrium isotope effects (EIEs) pertaining to isotopologues of $(silox)_2(^tBu_3SiNH)TiR$ (**1**-R), several conclusions can be reached. It is evident that modern ab initio methods, when applied to reasonable model complexes, are adequate for the calculation of EIEs. As a cautionary note, recognize that it is the special nature of equilibria of this type, and the generally appropriate application of the Born−Oppenheimer approximation, that renders each EIE subject to the calculation of only a single metal complex. Calculations of "normal" equilibria, i.e., **1′**-R + R′H ⇄ **1′**-R′ + RH (R, R′ are different hydrocarbyls), which require the calculation of two independent model complexes, are not nearly as energetically accurate.

Perhaps the most interesting consequence of this study concerns the importance of the MMI and EXC terms in the statistical mechanics formalism of the EIE (eq 4). Recall that in organic systems, both terms are typically neglected because of insignificant changes in mass and moment of inertia upon deuteration of large molecules, and because vibrational frequencies of organics are usually >500 cm^{-1}, rendering EXC contributions to EIE minimal. Generalizing from this work, it appears that the EXC and MMI terms can continue to be ignored, but for reasons that are significantly different. Both the MMI and EXC terms are substantial, but the latter—with help from components of the $EXP[-(\Delta\Delta ZPE/k_BT)]$ terms derived from low-frequency vibrations—attenuates the former to the extent that both can be neglected. It is the mass-dependent properties of the relatively small organic substrates in this study that constitute the MMI term, yet it is the low-energy vibrations of the metal complex that compensate for it via the EXC and $EXP[-(\Delta\Delta ZPE)/k_BT]$ terms. In a sense, it is the arbitrary way that the formalism in eq 4 partitions components of free energy that has led to some confusion regarding interpretation of EIEs. For example, if eq 4 had a rotational/vibrational partition function ratio instead of terms for rotation and vibration, the MMI component would not be distinct, etc.

From the perspective herein, $EXP[-(\Delta\Delta ZPE)/k_BT]$ terms, primarily bending vibrations, are the major contributors accounting for the magnitude of the EIEs and, presumably, corresponding KIEs. Uncorrelated bending modes—ones that are not common to metal complex and substrate—have proven to be the dominant factors in the generally greater magnitudes found for inter- vs intramolecular isotope effects. When comparing inter- and intramolecular isotope effects for the purpose of distinguishing mechanisms, these intrinsic differences must be carefully analyzed in order to avoid misinterpretation. As an additional cautionary note, cases can be deceptively complicated, and seemingly inconsequential vibrations can end up making substantial contributions. Furthermore, the greater variation and scope of vibrational frequencies encountered in transition metal systems, especially when different heteroatom−H/D bonds are exchanged, leads to isotope effects of greater magnitudes, and additional mechanistic hypotheses—such as light atom tunneling—need to be scrutinized with the utmost care before they are applied. In summary, it is safe to interpret EIEs, and presumably KIEs, through an understanding of zero-point energy differences, as long as the importance of bending vibrations is emphasized, but individual cases may manifest unexpected complications.

Experimental Section

General Considerations. All manipulations were performed using glovebox or high-vacuum techniques. Hydrocarbon and ethereal solvents were dried over and vacuum-transferred from sodium benzophenone ketyl. Benzene-d_6 was dried sequentially over sodium and 4-Å molecular sieves, and stored over and vacuum-transferred from sodium benzophenone ketyl. Cyclohexane-d_{12} was dried over sodium and then stored over and vacuum-transferred from Na/K alloy. All glassware was base-washed and oven-dried. NMR tubes for sealed tube experiments were flame-dried under active vacuum immediately prior to setup.

^1H NMR spectra were obtained using a Varian Unity 500 spectrometer; ^2H spectra were obtained on a Varian VXR-400S spectrometer equipped with a broad-band probe.

Cyclopropane-d_6 was purchased from CDN isotopes, Pointe-Claire, PQ, Canada. Lithium aluminum deuteride, iodoethane-2,2,2-d_3, cyclohexane-d_{12}, toluene-d_8, benzene-d_6, benzene-1,3,5-d_3, ethylene-d_4, ethylene-*trans*-1,2-d_2, ethane-d_6, and methane-d_n ($n = 2, 3, 4$) were ordered from Cambridge Isotope Laboratories, Andover, MA. Organotitanium compounds $(silox)_2(^tBu_3SiNH)TiR$ (**1**-R) were prepared as previously reported.[17]

Preparation of Deuterated Substrates. 1. Toluene-α-*d*. To a flask containing 20 mL of dry THF and 2.0 g of $LiAlD_4$ (0.047 mmol) at 0 °C was added 6.47 g (4.5 mL, 0.038 mmol) of benzyl bromide by syringe under Ar counterflow. The mixture was allowed to warm slowly to room temperature and stirred for 24 h. The flask was then transferred to a 14/20 distillation apparatus with a Vigreaux column, and THF was removed from the product by distillation under 1 atm of Ar. A fraction collected at 104 °C (~4 mL, 3.3 g) was found by ^1H NMR to be 95.6 mol % toluene-α-*d* and 4.4 mol % THF (89.1% yield of toluene-α-*d*, isotopic purity >99%). This mixture was dried over sodium and used without further purification in preparing the toluene intramolecular EIE samples.

2. Ethane-1,1,1-d_3. An oven-dried bomb reactor charged with 1.43 g of $LiAlH_4$ (0.038 mmol) was evacuated, and THF (20 mL) and CD_3CH_2I (1.5 mL, 0.019 mmol) were vacuum-distilled in at −78 °C. The mixture was stirred for 3 h, during which time it warmed slowly to room temperature. The bomb reactor was then degassed at −196 °C, warmed to −78 °C, and opened to another bomb reactor held at −196 °C, where the ethane-1,1,1-d_3 condensed. Further purification of the gaseous product was achieved by passing it through two −127 °C traps (1-propanol/liquid N_2), with the aid of a Toepler pump, and into a glass bomb reactor at −196 °C. ^1H NMR confirmed that the purified gas contained only CD_3CH_3 (septet, δ 0.77 (C_6D_6), $^3J_{HD}$ = 1.3 Hz). No other isotopologues could be observed, so isotopic purity was assumed to be >99%.

3. Cyclopropane-1,1-d_2. 1,1-Dibromocyclopropane (600 mg, 3.00 mmol), prepared by literature methods,[45] was introduced into an oven-dried glass bomb reactor, along with 1.80 g (6.16 mmol) of $^nBu_3SnD$ and 324 mg (1.97 mmol) of AIBN. Benzene (30 mL) was added by vacuum distillation, and the bomb reactor was heated at 60 °C for 24 h. After the reaction was done, the bomb was cooled to −196 °C and degassed. The solution was then warmed to room temperature, and cyclopropane-1,1-d_2 was isolated by trapping the solvent at −78 °C

(45) Seyferth, D.; Burlitch, J. M.; Minasz, R. J.; Mui, J. Y.; Simmons, H. D.; Treiber, A. J. H.; Dowd, S. R. *J. Am. Chem. Soc.* **1965**, *87*, 4259−4270.

Table 8. Initial Conditions ([**1**-R] in mM; R_HH, R_DD, or RH in equiv) for EIE Experiments Conducted via Schemes 1 and 2 and Eq 15[a]

1-R	substrate	[**1**-^{c}Pe]$_{init}$	[**1**−R_H]$_{init}$	[**1**-ND-R_D]$_{init}$	R_HH or RH	R_DD
			Intermolecular			
1-Me	CH_4/CD_4		68.2	22.8	2.6	2.6
	CH_4/CD_4		54.4	36.6	3.1	2.1
	CH_4/CD_4		61.1	29.9	1.7	3.5
1-Et	C_2H_6/C_2D_6		91.0	0	2.4	3.6
1-^{c}Pr	$^cC_3H_6/^cC_3D_6$	91.1	0	0	1.0	1.4
1-Vy	C_2H_4/C_2D_4	90.2	0	0	1.4	3.5
1-Ph	C_6H_6/C_6D_6	85.5	0	0	3.0	3.0
1-Bz	C_7H_8/C_7D_8		85.0	0	2.0	2.0
			Intramolecular			
1-Me	CDH_3	54.7			5.6	
	CD_2H_2	54.7			5.6	
	CD_3H	76.5			5.5	
1-Et	CD_3CH_3	91.0			6.2	
1-^{c}Pr	1,1-$^cC_3D_2H_4$	91.0			2.4	
1-Vy	*trans*-HDC═CHD	70.0			4.6	
1-Ph	1,3,5-$C_6D_3H_3$	73.8			6.6	
1-Bz	$PhCDH_2$	85.0			6.0	

[a] All at 26.5(3) °C except for **1**-Bz at 50.0(3) °C.

while passing the gaseous product, with the aid of a Toepler pump, through two additional cold traps (−100 °C) into the bomb reactor at −196 °C. The product was identified as cyclopropane-1,1-d_2 by ^{1}H NMR (quintet, δ 0.12 (C_6D_6), $^3J_{HD}$ = 1.2 Hz; isotopic purity >99%).

Kinetic Isotope Effect Measurements. C_6D_6 solutions of (silox)$_2$(^{t}Bu$_3$SiNH)TiR_H (**1**-R) and (silox)$_2$(^{t}Bu$_3$SiND)TiR_H (**1**-ND-R) were prepared in 2-mL volumetric flasks (66 mM; ∼95 mg/2 mL). Me_3-$SiOSiMe_3$ (∼1 mL) was added as an internal standard. Solutions were divided into three samples of 0.6 mL each using a 1-mL graduated pipet and transferred into flame-dried 5-mm NMR tubes which were fused to 14/20 joints and attached to needle valves. Each tube was degassed via three freeze−pump−thaw cycles and sealed under active vacuum. Both sets of tubes (**1**-R and **1**-ND-R) were kept in tandem at 26.5 °C in a Hewlett-Packard model 5890A gas chromatograph oven with the nominal temperature set to 25.0 °C (temperature was stable within ±0.3 °C). Rates of disappearance of ^{1}H resonances of hydrocarbyl groups were monitored by NMR (R = Et, Ti−CH_2 δ 1.97; R = CH═CH_2, TiCH_α δ 7.71; R = ^{c}Pr, *trans*-CH_β, δ 0.75). For R = Et and CH═CH_2, the elimination was monitored to five half-lives; for R = ^{c}Pr, poor baseline resolution in the cyclopropyl region resulted in unreliable integrals after two half-lives. Single transient spectra were used to obtain the most reproducible integrals. Rates and uncertainties were calculated from nonlinear, nonweighted least-squares fitting to the exponential form of the rate expression. In the case of **1**-^{c}Pr, one tube was lost, so statistics could not be calculated.

Equilibrium Isotope Effect Sample Preparation. 1. Intermolecular EIE Values. A 2-mL volumetric flask and a graduated pipet were employed to prepare 2.4-mL solutions of organotitanium compounds in C_6H_{12} (∼90 mM; 130−170 mg/2.4 mL). In the case of TiMe, mixtures of (silox)$_2$(^{t}Bu$_3$SiNH)TiMe (**1**-Me) and (silox)$_2$(^{t}Bu$_3$SiND)-TiCD_3 (**1**-ND-CD_3) were used (Table 8). Sufficiently pure samples of 1-CH═CH_2, **1**-^{c}Pr, and **1**-Ph could not be prepared due to the relatively fast hydrocarbon elimination rates of these compounds, so **1**-^{c}Pe was used as a precursor in these instances (eq 15). **1**-Et and **1**-Bz were the starting organometallics in the ethane and toluene EIE experiments, respectively. For experiments involving liquid hydrocarbon substrates (benzene and toluene), aliquots of perprotio and perdeuterio substrate were introduced into the sample solution at this point via microsyringe (Table 8). Solutions were divided into three 0.7-mL portions with a volumetric pipet and transferred to 5-mm NMR tubes fused to 14/20 joints. In the cases of the liquid substrates, tubes were simply attached to needle valves, freeze−pump−thaw degassed on a vacuum line, and sealed under active vacuum. For gaseous substrates, samples were attached to a three-tube adapter which was connected to two calibrated gas bulbs; solutions were freeze−pump−thaw degassed, and the entire apparatus was evacuated. Samples of R_HH and R_DD, accurately measured by manometer, were admitted into the two separate gas bulbs. Gases were purified by pumping off any noncondensables at −196 °C followed by warming and passing through a −78 °C trap. Needle valves between the two bulbs were opened, and the gases were allowed to mix for at least 1 h. The needle valve separating gas bulbs from samples was then opened, gases were allowed to condense for at least 1 h into the NMR tubes at −196 °C, and the tubes were flame-sealed under static vacuum. Quantities of gas were chosen to give a total substrate concentration (R_HH plus R_DD) of at least 90 mM in solution at equilibrium, taking into consideration Henry's law constants for each gas.[19] Tubes were kept at 26.5 °C in a Hewlett-Packard model 5890A GC oven in all cases except for **1**-Bz, in which instance tubes were held at 50.0 °C in a poly(ethylene glycol) bath with a Tamson immersion circulator.

2. Intramolecular EIE Values. For all substrates except the three methane isotopologues, solutions of (silox)$_2$(^{t}Bu$_3$SiNH)Ti^{c}Pe (**1**-^{c}Pe) in C_6D_{12} (2.4 mL, concentration variable; see Table 8) were prepared using a 2-mL volumetric flask and a graduated pipet. For the methane cases, the identical setup protocol was followed, but C_6H_{12} was used as a solvent. The solutions were divided into three 0.7-mL samples in NMR tubes sealed to 14/20 joints. Several equivalents of a partially deuterated hydrocarbon substrate (Table 8) were introduced either by microsyringe prior to transfer of samples to NMR tubes (benzene, toluene), or through the use of a calibrated gas bulb attached to a three-NMR-tube adapter holding the three sample tubes (gases were purified, admitted, and condensed as described for the intermolecular EIE experiments). Tubes were flame-sealed under active vacuum for liquid substrates and under static vacuum for gaseous substrates. Temperatures were regulated as specified for intermolecular EIE experiments.

Approach to Equilibrium Simulations. Kinetic simulations were performed for each EIE experiment prior to assay in order to predict when the system would attain equilibrium. Differential equations were written to describe the time-dependent change in concentration of each species in solution in terms of concentrations of organotitanium species and hydrocarbon substrates and rate constants for 1,2-RH-elimination and -addition. Rate constants were either experimentally measured (k_{elim}) or based on $\Delta G^\ddagger$ values calculated from estimates of the relative energies of **1**-R_H ground states, 1,2-RH-elimination/-addition transition states, and the putative (silox)$_2$Ti═NSi^{t}Bu$_3$ (**2**).[17] Kinetic isotope effects on 1,2-RH-addition were estimated using experimental elimination KIEs in conjuction with EIEs predicted by ab initio calculations (EIE = KIE_{addn}/KIE_{elim}). In Figure 9, sample simulations of the inter- (a) and intramolecular (b) EIEs pertaining to methane are illustrated. Reactions occurring in solution other than the 1,2-RH-elimination/-addition events of interest were also accounted for in the kinetic models (e.g., solvent activation, cyclopentane elimination from **1**-^{c}Pe, [2 + 2] addition of ethylene to **2** in the case of the **1**-CH═CH_2 experiments). Initial concentrations of organotitanium species and substrates used were identical to those used in actual experiments, and concentrations of gaseous substrates were estimated using Henry's law.[19] Numerical integration of differential equations for each kinetic model was performed using the EPISODE package for stiff functions.[46] The time at which the appropriate ratio of substrate and **1**-R_H/R_D/R concentrations fell within 1% of the predicted EIE was chosen as the starting point for assaying experiments.

EIE NMR Assay: Data Acquisition. 1. Intermolecular EIE Values. [**1**-R_H]/[R_HH] and [**1**-ND-R_D]/[R_DD] ratios were determined at equilibrium using ^{1}H and ^{2}H NMR spectroscopies, respectively. Use of a nondeuterated solvent (C_6H_{12}) was necessitated by the ^{2}H NMR experiments, so suppression of solvent signal was required during acquisition of ^{1}H NMR spectra. This was accomplished by saturating the C_6H_{12} resonance at δ 1.38 using either the proton decoupler channel during the d2 period (d2 = 1.5 s) or a 1.5 s transmitter presaturation. Shimming was performed by the following procedure. A sample in C_6D_{12} containing an amount of organotitanium compound similar to that used in the experiment of interest was shimmed using the standard solvent lock procedure. The solvent lock was then disabled, and fine shim adjustments were made on the intermolecular EIE sample by

(46) Byrne, G.; Hindmarsh, A. *EPISODE: An experimental package for the integration of systems of ordinary differential equations with banded Jacobians*; Lawrence Livermore Laboratory Report UCID-30132; Lawrence Livermore Laboratory: Livermore, CA, April 1976.

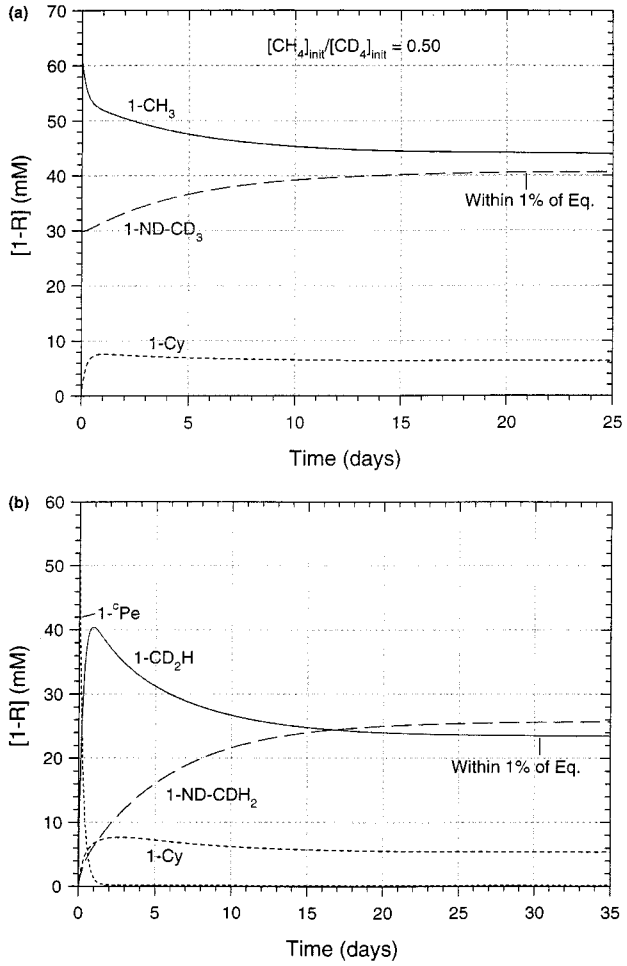

Figure 9. Simulations of the approach to equilibrium: (a) intermolecular methane case starting from **1**-CH_3 and **1**-ND-CD_3, and (b) intramolecular methane case starting from **1**-^{c}Pe and CH_2D_2.

observing solvent and ^{t}Bu ^{1}H resonances and adjusting shim parameters to optimize peak height and line shape. For each assay, ^{1}H and ^{2}H NMR spectra were acquired within 24 h of one another. Since reliable organotitanium-to-substrate ratios were critical, a number of precautions were taken in data acquisition to ensure the greatest possible accuracy of integrals. (a) A delay (d1) of at least 5 times the longest T_1 was used. T_1 values were measured for resonances of interest using the inversion recovery method, following calibration of a 90° pulse width for the signal. In all intermolecular EIE experiments, the longest T_1 values were those of the hydrocarbon substrates (Table 9.). T_1 values of substrates were measured in samples containing solely R_HH or R_DD hydrocarbon in C_6D_{12} or C_6H_{12}, respectively. (b) The spectral width was chosen so that all peaks were well within the transmitter range, thus avoiding attenuation of signals near the edge of the spectrum. The filter bandwidth was set to be identical to the spectral width (7000−10 000 Hz for ^{1}H; 3000 Hz for ^{2}H). (c) A pulse width slightly less than that of a 90° pulse was chosen (typically 8 μs for ^{1}H, 30 μs for ^{2}H). (d) Long acquisition times were used (6.0−8.5 s; spectral width dependent). (e) The number of data points was set to be large (128 000 for ^{1}H; 50 000 for ^{2}H), and zero-filling was employed by setting the Fourier number equal to the twice the number of points. (f) For ^{1}H NMR spectra, 32 transients were acquired; for ^{2}H spectra, acquisition was continued until a suitable signal-to-noise ratio was attained (80−500 transients; Table 9). (g) For ^{2}H NMR spectra, the ^{1}H decoupler was turned off during acquisition to avoid NOE distortion of signals.

2. Intramolecular EIE Values. With the exception of the three methane isotopologues, all intramolecular EIEs were assayed by ^{1}H NMR. The same data acquisition protocols were followed as in the ^{1}H portion of the intermolecular EIE experiments. Since C_6D_{12} solvent was used in these experiments, solvent suppression was not needed, and standard shim procedures were used. T_1 values for hydrocarbyl resonances of organotitanium species were measured directly in the EIE sample tubes (Table 9). Methane intramolecular EIEs were assayed by ^{2}H NMR. Shimming and data acquisition procedures were identical to those used in the ^{2}H portion of the intermolecular EIE experiments. For each assay, 800 transients were acquired.

EIE NMR Assay: Data Analysis. 1. Intermolecular EIE Values. During data workup, spectra were phased properly, and baseline corrections were employed prior to measurement of integrals. When possible, titanium−hydrocarbyl resonances were integrated to obtain organotitanium-to-substrate ratios in solution; in cases where hydrocarbyl resonances were obscured by the ^{t}Bu region or near the suppressed solvent peak, amide NH/D peaks were used. When calculating integral ratios of signals having significantly different line widths, integral cutoffs were chosen to be proportional to the half-height line widths of the peaks. Using $\int$ to indicate an NMR spectral integral, the assays were as follows:

(a) 1-(ND)-CD_3 + CH_4 ⇄ 1-CH_3 + CD_4. In the ^{1}H NMR spectrum, CH_4 (δ 0.11) and the NH (δ 7.16) of 1-CH_3 resonances were integrated. In the ^{2}H NMR spectrum, peaks corresponding to CD_4 (δ 0.09) and the $TiCD_3$ (δ 1.01) of **1**-(ND)-CD_3 were measured. $K_H/K_D = 3(\int NH/\int CH_4)(\int CD_4/\int TiCD_3)$.

(b) 1-(ND)-C_2D_5 + C_2H_6 ⇄ 1-C_2H_5 + C_2D_6. In the ^{1}H NMR spectrum, C_2H_6 (δ 0.77) and the NH (δ 7.00) of **1**-C_2H_5 resonances were integrated. In the ^{2}H NMR spectrum, peaks corresponding to C_2D_6 (δ 0.74) and the ND (δ 7.17) of **1**-(ND)-C_2D_5 were integrated. $K_H/K_D = (\int NH/\int C_2H_6)(\int C_2D_6/\int ND)$.

(c) 1-(ND)-^{c}C_3D_5 + ^{c}C_3H_6 ⇄ 1-^{c}C_3H_5 + ^{c}C_3D_6. ^{c}C_3H_6 (δ 0.14) and NH (δ 7.04) resonances were integrated in the ^{1}H NMR spectrum. ^{c}C_3D_6 (δ 0.10) and ND (δ 7.20) integrals were used in the ^{2}H NMR spectrum. $K_H/K_D = (\int NH/\int C_3H_6)(\int C_3D_6/\int ND)$.

(d) 1-(ND)-CD═CD_2 + C_2H_4 ⇄ 1-CH═CH_2 + C_2D_4. In the ^{1}H NMR spectrum, an average of the integrals of the three vinyl resonances (H_a, δ 7.43; H_b-*trans*, δ 5.97; $H_{b'}$-*cis*, δ 5.82) was used to represent **1**-CH═CH_2, and the C_2H_4 resonance (δ 5.25) was also integrated. Due to the broadness of the ^{2}H resonances, vinyl D_b-*trans* and $D_{b'}$-*cis* signals could not be resolved from the C_2D_4 resonance, and the vinyl D_a peak overlapped with the ND. The regions from 4.28 to 6.40 ppm (C_2D_4 + $D_{b,b'}$-*trans,cis*) and from 7.10 to 8.30 ppm (ND + D_a) were integrated in the ^{2}H NMR spectrum, and the integral ratio of C_2D_4 to **1**-(ND)-CD═CD_2 was calculated as $[\int(C_2D_4 + D_{b,b'}\text{-}trans,cis) - \int(ND + D_a)]/[\int(ND + D_a)/2]$. $K_H/K_D = [(\int H_a + \int H_b + \int H_{b'})/3)/\int C_2H_4][\int(C_2D_4 + D_{b,b'}\text{-}trans,cis) - \int(ND + D_a)]/[\int(ND + D_a)/2]$.

(e) 2-CD_2═CD_2 + C_2H_4 ⇄ 2-CH_2═CH_2 + C_2D_4. This EIE was obtained from the same ^{1}H and ^{2}H NMR spectra used in (d). In the ^{1}H NMR spectrum, the C_2H_4 resonance (δ 5.25) and the broad peak corresponding to the fluxional $-CH_2CH_2-$ bridge of the azametallacyclobutane (δ 3.04) were integrated. The ^{2}H NMR resonances integrated were the broad $-CD_2CD_2-$ resonance of the metallacycle at 3.02 ppm, and the C_2D_4 peak at 5.20 ppm, corrected for the overlapping **1**-(ND)-CD═CD_2 and $D_{b,b'}$-*trans,cis* resonances via subtraction as described above. $K_H/K_D = [\int(-CH_2CH_2-)/\int C_2H_4][(\int C_2D_4 + \int D_{b,b'}\text{-}trans,cis) - \int(ND + D_a)]/\int(-CD_2CD_2-)$.

(f) 1-ND-C_6D_5 + C_6H_6 ⇄ 1-C_6H_5 + C_6D_6. Integral ratios of the NH (δ 7.99) to C_6H_6 (δ 7.14) resonances were measured by ^{1}H NMR spectroscopy. In the ^{2}H NMR spectrum, ND and the *o*-D (2 H) phenyl resonances were unresolved, and the *m,p*-D (3 H) phenyl peaks overlapped with the C_6D_6 signal. Integrals were measured over the regions from 6.64 to 7.56 ppm (C_6D_6 + *m,p*-D) and from 7.70 to 9.20 ppm (ND + *o*-D), and the integral ratio of C_6D_6 to **1**-ND-C_6D_5 was computed as $[\int(C_6D_6 + m,p\text{-}D) - \int(ND + o\text{-}D)]/[\int(ND + o\text{-}D)/3]$. $K_H/K_D = [\int NH/\int C_6H_6][\int(C_6D_6 + m,p\text{-}D) - \int(ND + o\text{-}D)]/[\int(ND + o\text{-}D)/3]$.

(g) 1-ND-$CD_2C_6D_5$ + C_7H_8 ⇄ 1-$CH_2C_6H_5$ + C_7D_8. In the ^{1}H and ^{2}H NMR spectra, the methylene resonance at 3.06 ppm was used in correspondence to **1**-$CH_2C_6H_5$ and **1**-ND-$CD_2C_6D_5$, and the methyl peak (δ 2.21) was used for toluene and C_7D_8. $K_H/K_D = (\int TiCH_2Ph)(\int d_5\text{-}PhCD_3)/(\int TiCD_2Ph\text{-}d_5)(\int H_3CPh)$.

2. Intramolecular EIEs. The phasing, baseline correction, and integration procedures used in the intermolecular EIE experiments were also employed here.

Table 9. T_1 Values and Acquisition Parameters for EIE Observation by ^{1}H and ^{2}H NMR

1-R	substrate	longest ^{1}H T_1 (s) (resonance)	^{1}H NMR delay (s)	longest ^{2}H T_1 (s) (resonance)	^{2}H NMR delay (s)	^{2}H NMR transients
			Intermolecular[a]			
1-Me	CH_4/CD_4	18.1(1) (CH_4)	150	17(1) (CD_4)	86	80
1-Et	C_2H_6/C_2D_6	16(2) (C_2H_6)	100	8.5(7) (C_2D_6)	45	144
1-^{c}Pr	$^cC_3H_6/^cC_3D_6$	38(2) ($^cC_3D_6$)	210	4.44(4) ($^cC_3D_6$)	32	192
1-Vy	C_2H_4/C_2D_4	52(2) (C_2H_4)	300	13.3(5) (C_2D_4)	80	392
1-Ph	C_6H_6/C_6D_6	5.54(7) (C_6H_6)	60	1.468(6) (C_6D_6)	10	500
1-Bz	C_7H_8/C_7D_8	5.10(1) (C_7H_8 *p*-H)	60	4.9(1) ($-CD_3$)	30	196
			Intramolecular			
1-Me[a]	CDH_3 CD_2H_2 CD_3H			0.186(7) (CDH_3)	2	800
1-Et[b]	CD_3CH_3	1.95(6) ($TiCD_2CH_3$)	30			
1-^{c}Pr[b]	1,1-$^cC_3D_2H_4$	0.837(8) ($H_{\beta-trans}$)	30			
1-Vy[b]	*trans*-HDC=CHD	10.2(12) ($H_{\beta-trans}$)	80			
1-Ph[b]	1,3,5-$C_6D_3H_3$	17.8(4) (*p*-H)	95			
1-Bz[b]	$PhCDH_2$	1.47(4) (TiCDHPh)	30			

[a] C_6H_{12}; see text for solvent suppression information. [b] C_6D_{12}.

(a) 1-ND-CH$_x$D$_{3-x}$ ⇄ 1-CH$_{x-1}$D$_{4-x}$ (x = 1−3). For all three sets of experiments, the ^{2}H resonances of the methyl groups of both isotopomers appeared as one broad peak centered between 1.04 and 1.08 ppm. The integrations of this peak and the ND resonance (δ 7.32), with appropriate symmetry factors, were used to calculate K_H/K_D for each case according to the following formulas: CH_3D (x = 3), $K_H/K_D = \{\int TiCH_2D/\int ND\}$; CH_2D_2 (x = 2), $K_H/K_D = (\int(TiCHD_2 + TiCH_2D) - \int ND)/2\int ND$; CHD_3 (x = 1), $K_H/K_D = \{(\int(TiCHD_2 + TiCD_3) - 2\int ND)/3\int ND\}$.

(b) 1-ND-CD$_2$CH$_3$ ⇄ 1-CH$_2$CD$_3$. The methylene resonance of **1**-CH_2D_3 (δ 1.78) and the methyl resonance of **1**-ND-CD_2CH_3 (δ 1.56) were integrated in the ^{1}H NMR spectrum. $K_H/K_D = (\int CH_2/2)/(\int CH_3/3)$.

(b) 1-ND-^{c}C$_3$H$_4$D ⇄ 1-^{c}C$_3$H$_3$D$_2$. An unresolved multiplet from 0.65 to 0.70 ppm in the ^{1}H NMR spectrum contained the H$_b$-*trans* signals for both isotopomers. This multiplet and the NH peak (δ 7.10) were integrated to obtain the EIE: $K_H/K_D = \{\int NH/[(\int H_b\text{-}trans\text{-}\int NH)/2]\}$.

(c) 1-ND-*trans*-CH=CHD ⇄ 1-trans-CD=CHD. The vinyl H$_b$-*trans* resonance at 6.00 ppm served as a ^{1}H NMR spectral handle on 1-*trans*-CD=CHD, while an average of the integrations of the vinyl H$_b$-*cis* (δ 5.86) and H$_a$ (δ 7.49) peaks was used as to represent **1**-ND-*trans*-CH=CHD. $K_H/K_D = \int H_b\text{-}trans/[(\int H_b\text{-}cis + \int H_a)/2]$.

(d) 1-ND-3,5-C$_6$H$_3$D$_2$ ⇄ 1-2,4,6-C$_6$H$_2$D$_3$. ^{1}H NMR spectral handles used were the sum of the NH (δ 8.07) and *m*-phenyl (δ 6.96) resonances for **1**-2,4,6-$C_6H_2D_3$, and the sum of the *p*- (δ 7.01) and *o*-phenyl (δ 7.92) resonances for **1**-ND-3,5-$C_6H_3D_2$: $K_H/K_D = (\int NH + \int m\text{-}H)/(\int o\text{-}H + \int p\text{-}H)$.

(e) 1-ND-CH$_2$Ph ⇄ 1-CHDPh. The methylene resonances for the two isotopomers were well resolved (δ 3.11 for **1**-ND-CH_2Ph, δ 3.09 for **1**-CHDPh) in the ^{1}H NMR spectrum. These peaks were integrated to calculate the EIE: $K_H/K_D = \{\int TiCHDPh/(\int TiCH_2Ph/2)\}$.

GAMESS Calculations. The ECPs of Stevens et al.[47] replace the innermost core orbitals for TMs and all core orbitals for main-group (MG) elements. Thus, the *n*s, *n*p, *n*d, (n + 1)s, and (n + 1)p are treated explicitly for TMs; for the main group, *n*s and *n*p are treated explicitly. Transition metal ECPs are created from *all-electron* Dirac−Fock calculations and thus include Darwin and mass velocity relativistic effects.[47] The effect of electron correlation on optimized geometries is expected to be minimal because of the empty d shell in the complexes studied.[48,49] The Stevens valence basis set (VBS) is quadruple and triple-ζ for the sp and d manifolds, respectively, for transition metals. For MG elements the VBS is double-ζ-plus-polarization.

All systems studied are closed-shell singlets that are geometry optimized at the restricted Hartree−Fock level of theory with the ECP/VBS combinations outlined above. This level of theory, termed RHF/SBK(d), has been shown in many previous studies to very accurately describe the structure and bonding of TMs in diverse chemical environments.[48,49] The energy Hessians (second derivative of the energy with respect to the atomic coordinates) are calculated at $(HO)_2(H_2N)$-TiR (**1′**-R) stationary points by numerical double differentiation of analytical gradients. Computed thermodynamic quantities[50] used in the calculation of thermodynamic quantities were determined at the RHF level using the unscaled vibrational frequencies derived from the energy Hessian. Corrections for the zero-point energy and from absolute zero to 297.95 K are added as needed. In a previous study, Raby and Cundari showed the RHF/SBK(d) scheme generated TM−ligand stretching frequencies with commensurate accuracy to that seen employing all-electron methods on organic molecules.[51] Calculations utilized the GAMESS and parallel-GAMESS programs on several platforms: SP-2 (San Diego); IBM RISC 6000 (Memphis); SGI O2, Origin 2000 and Octane (Memphis).[52] Figures were constructed with the aid of MacMolPlt.[53]

Acknowledgment. We thank the National Science Foundation, Cornell University, and University of Memphis for support of this research, Alan S. Goldman, Benjamin Widom, and Barry K. Carpenter for helpful comments, and Jordan L. Bennett and Cathy C. Lester for experimental assistance.

Supporting Information Available: Vibrational frequencies and their contributions via EXC and EXP[$-(\Delta\Delta ZPE/k_BT)$] terms for all **1**-R_H, R_HH, **1**-ND-R_DD, R_DD, **1**-R, and **1**-ND-R′ according to the various inter- and intramolecular isotopic equilibria (e.g., Table 3) (PDF). This material is available free of charge via the Internet at http://pubs.acs.org.

JA000112Q

(47) (a) Stevens, W. J.; Krauss, M.; Basch, H.; Jasien, P. G. *Can. J. Chem.* **1992**, *70*, 612−630. (b) Stevens, W. J.; Basch, H.; Krauss, M. *J. Chem. Phys.* **1984**, *81*, 6026−6033.

(48) Cundari, T. R.; Benson, M. T.; Lutz, M. L.; Sommerer, S. O. In *Reviews in Computational Chemistry*; Boyd, D. B., Lipkowitz, K. B., Eds.; VCH: Weinheim, 1996; Vol. 7, p 145.

(49) Cundari, T. R.; Gordon, M. S. *Coord. Chem. Rev.* **1996**, *147*, 87−115.

(50) Hehre, W. J.; Radom, L.; Schleyer, P. v. R.; Pople, J. A. *Ab Initio Molecular Orbital Theory*; Wiley: New York, 1986.

(51) Cundari, T. R.; Raby, P. D. *J. Phys. Chem. A* **1997**, *101*, 5783−5788.

(52) Schmidt, M. W.; Baldridge, K. K.; Boatz, J. A.; Elbert, S. T.; Gordon, M. S.; Jensen, J. H.; Koseki, S.; Matsunaga, N.; Nguyen, K. A.; Su, S. J.; Windus, T. L.; Dupuis, M.; Montgomery, J. A. *J. Comput. Chem.* **1993**, *14*, 1347−1363.

(53) Bode, B. M.; Gordon, M. S. *J. Mol. Graphics Mod.* **1998**, *16*, 133−138.